Chemical Papers
https://doi.org/10.1007/s11696-026-04771-z

ORIGINAL PAPER

Synthesis, enzyme inhibition, in silico molecular docking and DFT analysis of novel multi-functionalized thiourea and thiazolidinone benzenesulfonamides

Mehtap Tugrak Sakarya[1] · Cem Yamali[2] · Adem Erturk[3] · Yusuf Sert[4] · Halise Inci Gul[5] · Mustafa Gul[6] · Ilhami Gulcin[3]

Received: 3 January 2025 / Accepted: 25 February 2026
© The Author(s) 2026

Abstract

Enzymes play important roles in various physiological processes, and dysregulation of enzyme expression is linked to the onset and progression of many diseases, including Alzheimer's disease and diabetes. Enzyme-targeted therapies are promising in the treatment of enzyme-related diseases, making enzymes both biomarkers and targets for therapeutic investigations. In this study, the synthesis and biological assessment of novel multi-functionalized thiourea and thiazolidinone benzenesulfonamides were reported along with their CAs inhibition, AChE inhibition, α-glucosidase, and α-amylase inhibitions. While compound **M1**, which had a Ki value of 19.88 ± 1.04 nM (hCA I), was found to be the most potent hCA I inhibitor, compound **M9**, which had a Ki 8.9890 ± 0.8909 nM was found to be the strongest inhibitor against hCA II. Compound **M1** showed remarkable AChE inhibition effects with a Ki value of 0.4740 ± 0.0818 nM in comparison to tacrine. The compounds showed Ki_s in the range of 4.9395 ± 0.8288 – 46.1207 ± 19.5197 nM against α-glycosidase and IC_{50} values in the range of 12.044 – 56.533 nM against α-amylase. In addition, molecular docking studies were performed to examine and evaluate the interaction of the lead compounds against the enzymes studied. The binding energy values and predicted inhibition constants (Ki) support the effectiveness of these molecules, aligning closely with experimental findings. These results highlight the robustness of the computational approach in identifying potential inhibitors and provide critical insights into the structure-activity relationships, aiding future drug development and therapeutic research.

Keywords Benzenesulfonamide · Thiourea · Thiazolidinone · Carbonic anhydrase · Acetylcholinesterase · Molecular docking

✉ Mehtap Tugrak Sakarya
mehtaptugrak@hotmail.com; mehtap.tugrak@gop.edu.tr; mehtaptugrak@gmail.com

[1] Department of Pharmaceutical Chemistry, Faculty of Pharmacy, Tokat Gaziosmanpasa University, Tokat, Turkey

[2] Department of Basic Pharmaceutical Sciences, Faculty of Pharmacy, Cukurova University, Adana, Turkey

[3] Department of Chemistry, Faculty of Science, Ataturk University, Erzurum, Turkey

[4] Department of Motor Vehicles and Transportation Technologies, Sorgun Vocational High School, Yozgat Bozok University, Yozgat, Turkey

[5] Department of Pharmaceutical Chemistry, Faculty of Pharmacy, Ataturk University, Erzurum, Turkey

[6] Department of Physiology, Faculty of Medicine, Ataturk University, Erzurum, Turkey

Abbreviations

CA	Carbonic anhydrase
AChE	Acetylcholinesterase
hCA I	Human carbonic anhydrase I
hCA II	Human carbonic anhydrase II
NMR	Nuclear magnetic resonance
HRMS	High resolution mass spectrometry
AZA	Acetazolamide
AD	Alzheimer disease
ACh	Acetylcholine
Ch	Choline
T2DM	Type 2 diabetes mellitus
TAC	Tacrine
ACR	Acarbose
DMSO	Dimethyl sulfoxide
KSCN	Potassium thiocyanate

Published online: 07 April 2026

EtOH	Etanol
DFT	Density functional theory
MEP	Molecular electrostatic potential

Introduction

Alzheimer's disease (AD) poses significant and growing global concerns as the most common form of dementia. The exact mechanisms behind Alzheimer's disease are still not fully known, and the etiology of the disease is varied (Arif et al. 2024). In addition to the Aβ and tau protein hypothesis, a variety of other factors can play a role in the development of AD. These include impairments in acetylcholine, inflammation of the nervous system, oxidative stress, imbalance of glutamate and biometal homeostasis, insulin resistance, etc. (Zhang et al. 2024). One of the most efficacious treatments for AD that has been discovered to date is the inhibition of acetylcholinesterase (AChE; E.C.3.1.1.7) (Marucci et al. 2021). Galantamine, rivastigmine, and donepezil, and their combinations are frequently utilized as acetylcholinesterase inhibitors (AChEIs). Despite the extensive use of these drugs, ongoing research is directed towards optimising dosage, dosage form, routes of administration, and combination therapies with the objective of minimising adverse effects. These medications are useful for developing future medications because they mainly work by influencing neurotransmitter levels; nevertheless, they are unable to change the disease's progression (Zhang et al. 2024; Nunes et al. 2022; Azhar Hussain et al. 2023). Additionally, it has been stated that Aducanumab, Lecanemab, and Donanemab are novel medications that are currently undergoing clinical trials. In terms of clearing Aβ plaque and reducing cognitive decline, all three have demonstrated their effectiveness. However, it is important to highlight that the risks of amyloid-related imaging abnormalities and the expenses associated with their treatment (Zhang et al. 2024). Semagacestat (LY-450139), Avagacestat (BMS-708163) were reported as γ-secretase inhibitors. However, participants experienced adverse reactions such as gastrointestinal symptoms, skin cancer (Yang et al. 2021; Gupta et al. 2013; Coric et al. 2015). Then, researchers have explored inhibiting β-secretase (BACE1) as an alternative to γ-secretase inhibitors due to its higher selectivity for amyloid-beta precursor protein (APP), aiming to reduce Aβ production. Umibecestat (CNP520) and Elenbecestat (E2609) were reported a fourth-generation BACE1 inhibitors under clinical studies (Imbimbo and Watling 2019). As can be seen, while drugs with different mechanisms of action continue to be used in the clinic, clinical trials and studies on the discovery of new drug candidates with different mechanisms of action continue intensively due to the inadequacy of existing drugs (Imbimbo and Watling 2019).

Type 2 diabetes mellitus (T2DM) is a complex and persistent metabolic disorder triggered by insulin resistance in cells of the body (Hayat et al. 2023; Iqbal et al. 2025). T2DM is characterized by postprandial hyperglycemia. Treatments aimed at enhancing postprandial glycemia by decreasing glucose intake from digestible carbs were recommended to early-stage diabetic patients prior to the initiation of pharmacological treatments (Ch'ng et al. 2019; Hayat et al. 2023; Iqbal et al. 2025). A therapeutic approach for T2DM involves restricting intestinal glucose absorption by inhibiting the enzymes α-amylase and α-glucosidase, which hydrolyze carbs (Saltos et al. 2015). α-Amylase and α-glucosidase inhibitors, which prevent glucose from entering the circulation by slowing carbohydrate digestion, are considered as a preventive treatment of hyperglycaemia (Chiasson et al. 2002). Clinically approved α-glucosidase inhibitors, such as acarbose, also block α-amylase. Acarbose is widely administered but requires carbohydrate co-administration to reduce hypoglycemia. This treatment can cause gastrointestinal side effects (Kokil et al. 2010). In addition, thiazolidinediones and sulfonylureas are drug groups that have been used for many years in the treatment of diabetes mellitus. Thiazolidinediones (TZDs), such as pioglitazone and rosiglitazone (Fig. 1), are a class of medications. Studies show that TZDs can lead to improved glycemic control, reduced insulin resistance, and potential benefits on lipid profiles. However, concerns exist regarding weight gain, heart failure risk, and potential bone fractures (Christos et al. 2016; Nanjan et al. 2018). On the other hand, sulfonylureas, including glimepiride and glyburide (Fig. 1), stimulate insulin release from pancreatic beta cells. They are effective in lowering blood glucose levels, particularly in patients with T2DM. Long-term use may also be associated with a gradual decrease in effectiveness due to beta-cell exhaustion (Douros et al. 2017; Mary and Korytkowski 2004). Both thiazolidinediones and sulfonylureas play important roles in managing type 2 diabetes, each with distinct mechanisms, benefits, and risks (Rizos et al. 2016). Consequently, numerous studies have focused on creating novel and efficient alternatives, covering various categories of natural compounds and a range of synthetic compounds. Therefore, pharmaceutical studies on antidiabetic drugs continue to optimise the side effect profile and patient outcomes.

Carbonic anhydrases (CAs, EC 4.2.1.1) are metalloenzymes that operate as efficient catalysts for the reversible hydration of carbon dioxide into bicarbonate which play important physiological functions in lipogenesis, gluconeogenesis, ureagenesis, and tumorigenicity. Carbonic anhydrase inhibitors (CAIs) also have therapeutic uses for

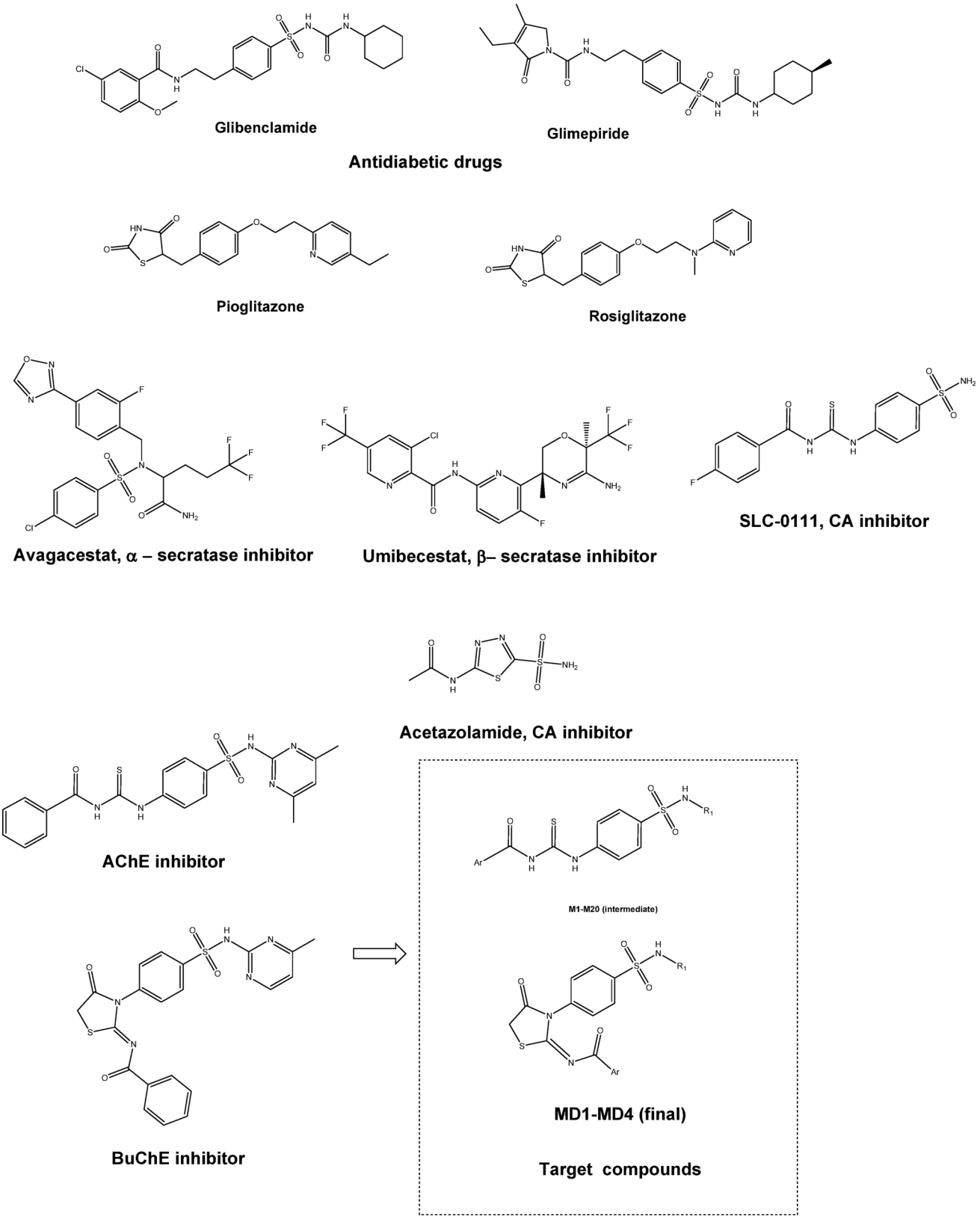


Fig. 1 Chemical structure of the representative compounds (Tugrak Sakarya et al. 2023), drugs and target compounds

the treatment of many clinical diseases. Several major sulfonamides and their derivatives are recognized as versatile class of CA inhibitors. Well-known sulfonamide-based CA inhibitors are acetazolamide (AZA, Fig. 1), ethoxzolamide, and methazolamide, etc. (Alterio et al. 2012; Neri and Supuran 2011; Supuran 2018; Carta et al. 2014). In addition, SLC-0111 (Fig. 1) has garnered attention due to its specific inhibitory effect on cancer-associated CA isoforms IX and XII. SLC-0111 exhibited significant anticancer and antimetastatic properties in animal models (Lou et al. 2011; Pacchiano et al. 2010, 2011). However, their therapeutic application is frequently limited by undesirable adverse effects, including paresthesia, fatigue, gastrointestinal disturbances, metabolic acidosis, nephrolithiasis, and in rare cases, severe hypersensitivity reactions (Alterio et al. 2012; Neri and Supuran 2011; Supuran 2018; Carta et al. 2014). Beyond their established physiological roles, emerging evidence suggests that specific carbonic anhydrase isoforms may also be implicated in neurodegenerative processes. Recent studies have demonstrated that pharmacological inhibition of mitochondrial carbonic anhydrases can attenuate amyloid-β-induced mitochondrial dysfunction and neurovascular toxicity, indicating a potential role of CA modulation in Alzheimer's disease pathology. Furthermore, CA inhibition has been associated with the regulation of oxidative stress and neuroinflammatory responses, both of which are key contributors to AD progression (Solesio et al. 2018; Lemon et al. 2021; Lopez et al. 2025). In addition, their limited isoform 5selectivity contributes to off-target effects and variable patient tolerability. These safety and pharmacological limitations highlight a clear unmet need for the development of novel carbonic anhydrase inhibitors with improved selectivity, enhanced safety profiles, and optimized pharmacokinetic properties (Alterio et al. 2012; Neri and Supuran 2011; Supuran 2018; Carta et al. 2014).

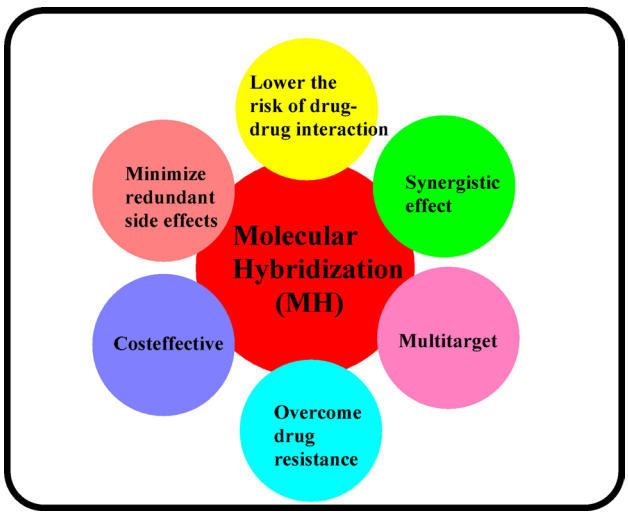


Fig. 2 The importance of molecular hybridization (Buchanan et al. 2023)

Molecular hybridization (MH) is a drug design approach that enables rational drug design to create new hybrid molecules by covalently combining pharmacophoric moieties from various bioactive chemicals (Khan et al. 2024). In general, combining molecular motifs with different pharmacological activities can produce compounds with altered selectivity profiles, different and/or dual modes of action, fewer side effects, the ability to overcome multidrug resistance, and an improved safety profile Fig. 2 (Viegas-Junior et al. 2007; Khan et al. 2023a). In recent years, multitarget-directed ligand (MTDL) strategies have gained considerable attention for the treatment of multifactorial disorders such as Alzheimer's disease and T2DM. The integration of complementary pharmacophoric elements within a single molecular scaffold has been proposed as a rational approach to simultaneously modulate distinct biological targets involved in complex pathologies (Mesiti et al. 2019; Pathak and Kabra 2024).

Based on this concept, in this study, substituted-sulfonamide, thiazolidinone, and thiourea/acylthiourea pharmacophores are considered to design hybrid molecules. Sulfonamides are essential groups in drug development since they exhibit a diverse range of activities, including antidiabetic, AChE inhibition, CA inhibition, and anticancer (Tugrak et al. 2020, 2021a, b; Yamali et al. 2023; Tugrak Sakarya et al. 2023; Zada et al. 2022). Thiazolidinone ring has received a great deal of attention over the years since it is a significant and versatile moiety to design bioactive compounds, including antidiabetic, anti-Alzheimer's disease, and CA inhibitory activities (Tugrak Sakarya et al. 2023; Gamal et al. 2024; Khan et al. 2023b; Ullah et al. 2022). When the chemical structures of antidiabetic drugs pioglitazone and rosiglitazone given in Fig. 1 are analysed, the thiazolidinone ring, pyridine skeleton, and the etheric chain group connecting these two groups draw attention, while when the chemical structures of Glimepiride and glyburide drugs are considered, arylbenzamide and sulfamoylurea groups draw attention. It may show that these groups are important groups that play a role in the antidiabetic effect of drugs (Tugrak Sakarya et al. 2023; Gamal et al. 2024; Khan et al. 2023b; Ullah et al. 2022).

Thiourea has also gained interest due to its numerous applications and biological significance. It has a variety of biological activities, including anti-diabetic, anti-Alzheimer's disease, CA inhibitory, etc. Tugrak et al. 2020, 2021c; Khan et al. 2022; Aleid et al. 2024). Moreover, acylthiourea derivatives have garnered significant interest in pharmaceutical research owing to their remarkable bioactivity and their role as intermediates in the synthesis of several pharmacophore groups (Zahra et al. 2022). Compounds featuring the

acylthiourea moiety exhibit many pharmacological activities, including antiviral, anticancer, anti-inflammatory, and antidiabetic actions through the inhibition of α-amylase and α-glucosidase (Khan et al. 2022; Kulabaş et al. 2017; Efeoglu et al. 2022). Thiourea and its derivatives have also shown potential in the context of Alzheimer's disease due to their ability to inhibit certain enzymes and modulate biochemical pathways associated with the disease. Our investigation documented acylthiourea-based compounds (Fig. 1) exhibiting in vitro inhibitory effects against acetylcholinesterase and butyrylcholinesterase. The results indicated that the compounds had superior efficacy against AChE compared to BuChE (Tugrak Sakarya et al. 2023).

Based on previous studies, we considered substituted sulfonamide, thiazolidinone, and thiourea/acylthiourea pharmacophores for the construction of hybrid molecules. Intermediate compounds bearing arylamide, thiourea, and sulfonamide residues, and final compounds bearing a substituted thiazolidinone ring and pyrimidine-substituted sulfonamide moiety were rationally designed by the hybridization of structural motifs present in clinically relevant drug molecules and our previous studies. In the first stage of the design, these hybrids were primarily expected to show α-amylase and α-glucosidase inhibitory potential. In a second step, based on our previous findings demonstrating the relevance of thiourea/acylthiourea derivatives in the context of Alzheimer's disease, the designed compounds were also evaluated as acetylcholinesterase inhibitors. Finally, considering their structural similarity to reference carbonic anhydrase inhibitors such as SLC-0111, which possess thiourea and sulfonamide functionalities, the designed hybrids were anticipated to exhibit carbonic anhydrase inhibitory activity.

Although acetylcholinesterase and carbonic anhydrases possess distinct catalytic architectures, the simultaneous evaluation of these enzymes in the present study is based on the multifactorial nature of Alzheimer's disease rather than structural similarity between their active sites. While AChE inhibition primarily addresses cholinergic neurotransmission deficits and provides symptomatic relief, emerging evidence indicates that modulation of specific CA isoforms may influence amyloid-β accumulation, mitochondrial dysfunction, oxidative stress, and neuroinflammatory processes (Tugrak et al. 2021a; Neri and Supuran 2011; Supuran 2018; Tugrak et al. 2020).Therefore, targeting these enzymatic systems within the same chemical framework may contribute to both symptomatic and disease-related mechanisms.

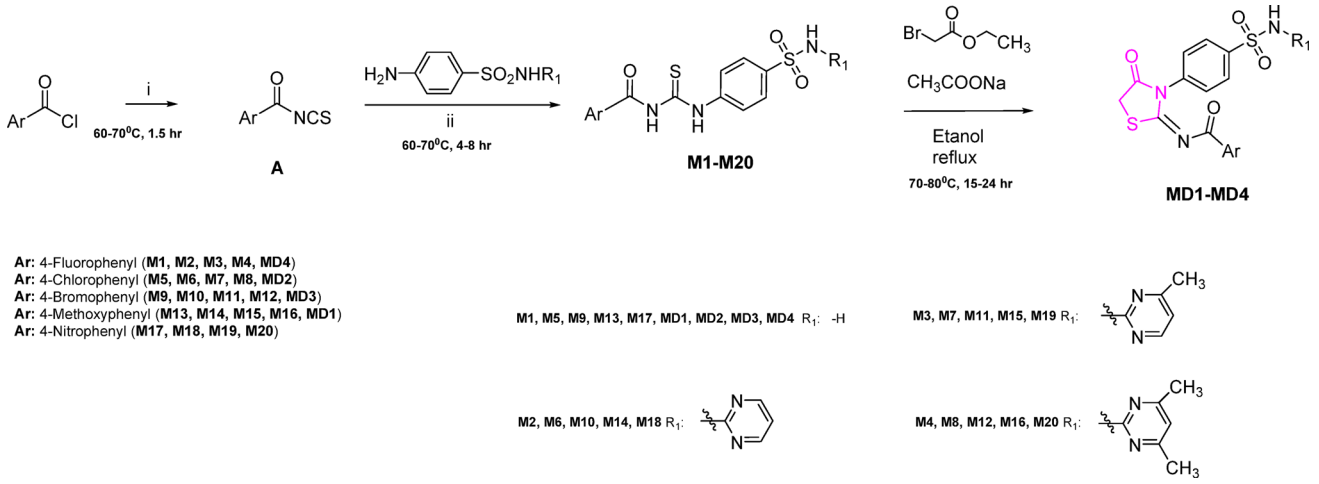
In parallel with this scaffold selection, a rational molecular hybridization strategy was deliberately employed by integrating multiple privileged pharmacophoric motifs into a single chemical framework. Thiazolidinone, thiourea, and acylthiourea scaffolds were selected based on their well-documented enzyme inhibitory potential and favorable binding characteristics reported in the literature. This hybrid design approach was intended to enhance binding efficiency, broaden the inhibitory spectrum, and improve structure-based complementarity toward the active sites of carbonic anhydrase, acetylcholinesterase, α-glucosidase, and α-amylase. In this research, the synthesized compounds were subsequently evaluated in vitro against AChE, α-amylase, α-glucosidase, hCA I, and hCA II, and complemented by in silico molecular docking studies to elucidate binding modes and rationalize the observed inhibition profiles.

Results and discussion

Chemistry

Compounds bearing benzamide, thiourea, and sulfonamide residues and substituted thiazolidine rings are known to possess a wide range of biological activities according to our previous studies (Tugrak et al. 2020; Tugrak Sakarya et al. 2023). First, 20 compounds (**M1-M20**) were designed and synthesized. The synthetic route is illustrated in Scheme 1. Carbonyl isothiocyanate derivatives **A** were synthesized by nucleophilic substitution reaction between commercially available substituted benzoyl chloride and potassium thiocyanate. Then, the title compounds **M** were prepared by an addition-elimination reaction. Through effective combinations of twenty carbonyl isothiocyanate (**A**) and four commercially substituted sulfonamide derivatives, title compounds (**M1-M20**) were obtained. A common synthetic strategy to construct imino thiazolidinones (**MD1-MD4**) relies on cyclization of thioureas with acids in the presence of an inorganic base (i.e., NaOAc) in polar solvents such as ethanol. In this study, in order to synthesize thiazolidinones, a three-step reaction procedure was involved. The novel sulfonamide-based thiazolidinone derivatives (**MD1-MD4**) were synthesized using the method outlined in Scheme 1.

In the first step, aroyl isothiocyanate derivatives were synthesized by the reaction of aroyl chlorides (4-fluorobenzoyl chloride for **M1-M4**, **MD4**, 4-chlorobenzoyl chloride for **M5-M8**, **MD2**, 4-bromobenzoyl chloride for **M9-M12**, **MD3**, 4-methoxybenzoyl chloride for **M13-M16**, **MD1** and 4-nitrobenzoyl chloride for **M17-M20** series) and potassium thiocyanate in acetone (Scheme 1). It was refluxed for 1.5 h at 60 – 70 °C, continuously stirring. The intermediate was collected by filtration and recrystallized from ethanol. Then, aroyl isothiocyanates were reacted with substituted sulfonamides (sulfanilamide, sulfadiazine, sulfamerazine, and sulfamethazine) to obtain compounds **M1-M20**. This reaction was carried out in the presence of acetone for 4 – 8 h. The resulting precipitate was collected by filtration



Scheme 1 General synthesis of compounds (**M1-M20**, **MD1-MD4**). (i) KSCN, acetone, reflux 1.5 h, 60 – 70 °C; (ii) acetone, reflux, 4 – 8 h, 60 – 70 °C. (iii) Etanol, reflux, 70-80°C, 15-24h

and recrystallized from dimethylformamide/ethanol/H_2O (4.2:0.6:0.2) to obtain the pure products **M1-M20**. Finally, ethyl bromoacetate and sodium acetate were added to the solution of benzamide derivatives (**M1-M20**), stirred in acetone, and refluxed for 15 – 24 h to obtain the targeted thiazolidinone derivatives (**MD1-MD4**) (Scheme 1). The relatively low isolated yields obtained for the thiazolidinone derivatives (**MD1-MD4**) can be attributed to several experimental challenges. The cyclization step was found to be sensitive to both solvent system and thermal conditions, and prolonged heating led to the formation of side products, as evidenced by highly complex thin layer chromatography (TLC) profiles. In addition, the limited solubility of the intermediate benzamide/thiourea precursors in acetone adversely affected reaction homogeneity and conversion efficiency. Although various reaction parameters were screened to improve the yields, these intrinsic limitations of the cyclization process prevented significant yield enhancement. Therefore, future studies will focus on alternative solvents and milder cyclization strategies to increase the efficiency of thiazolidinone formation. When the reaction was completed, the precipitates formed were filtered and recrystallized from ethanol to afford the products (**MD1-MD4**). All compounds **M1-M20** and **MD1-MD4** were characterized by spectral methods such as ^{1}H NMR, ^{13}C NMR, and HRMS.

When the ^{1}H NMR spectra of the **M1-M20** compounds were examined, the proton signals belonging to the NH groups of the urea function were observed in the range of δ 12.93 –12.43 ppm and 12.03 –11.49 ppm. Aliphatic and aromatic protons were seen to be compatible with the structure. While the methyl protons belonging to the sulfamerazine structure were observed in the range of δ 2.31– 2.33 ppm, the sulfamethazine structure showed characteristic signals resonating in the aliphatic range δ 2.25 – 2.32 ppm, attributable to the methyl groups of $(CH_3)_2$. ^{13}C NMR spectra revealed that aryl and aliphatic carbon peaks of the compounds were observed in the expected areas. ^{13}C NMR spectra of compounds (**M1-M20**) revealed the presence of the signal of the sulfonyl carbon (C=S) in the range δ 179.1-179.9 ppm, whereas the signals due to the carbonyl carbon (C=O) appeared δ 166.7-168.8 ppm. High-resolution mass spectrometry (HRMS) data also confirmed the molecular structure of the compounds.

Inhibitory potency of the compounds towards CAs

The synthesized compounds were evaluated in vitro against hCA I and hCA II enzymes. hCA I was inhibited by thiourea-substituted benzenesulfonamides **M1-M20** with Ki values ranging from 19.88 ± 1.04 nM to 60.5649 ± 18.1635 nM. Additionally, many compounds exhibited higher inhibitory potency against hCA I in comparison to the reference inhibitor AZA (Ki = 36.3990 ± 9.0100 nM).

The compound, 4-fluoro-*N*-((4-sulfamoylphenyl)carbamothioyl)benzamide (**M1**), (Table 1) was the most potent inhibitor of hCA I with a Ki of 19.88 ± 1.04 nM, the second most potent inhibitor was analog **M10** with a Ki of 22.2169 ± 2.1601 nM, derivative **M7** was the third most potent inhibitor with a Ki of 23.0232 ± 4.6367 nM. The inhibitory activities of the thiourea-substituted benzenesulfonamides against CA I followed the decreasing order of **M1 > M10 > M7 > M5 > M12 = M13 > M9 > M8 > M16 > M19 > M3 > M18 > M11 > M2 > M20 > M6 > M14 > M4 > M17 > M15.**

Different inhibition data are obtained depending on the linker found in the compounds. When thiazolidinone derivatives (**MD1-MD4**) are synthesized starting from thiourea-substituted benzenesulfonamides, group-dependent changes occur in hCA I enzyme inhibition results. According to the

Table 1 Carbonic anhydrase (CAs) and Acetylcholinesterase (AChE) inhibition results of the compounds **M1-M20**

Compounds	IC_{50} (nM)						Ki (nM)		
	AChE	r^2	hCA I	r^2	hCA II	r^2	AChE	hCA I	hCA II
M1*	3.629	0.989	24.75	0.9718	25.67	0.9869	0.4740 ± 0.0818	19.88 ± 1.04	49.86 ± 6.18
M2*	4.8471	0.9816	30.13	0.9804	31.50	0.9729	0.5889 ± 0.0145	45.20 ± 1.24	18.92 ± 1.63
M3*	4.2786	0.9864	33.00	0.9834	30.13	0.9741	0.8087 ± 0.1925	30.17 ± 2.35	8.15 ± 1.50
M4*	3.7467	0.9911	29.87	0.9952	26.65	0.9801	0.5681 ± 0.03136	55.95 ± 10.72	47.96 ± 7.91
M5	5.5452	0.9892	34.6574	0.997	38.5082	0.9903	1.0147 ± 0.1725	24.0673 ± 1.9530	32.4192 ± 7.1743
M6	3.5185	0.9893	53.319	0.998	57.7623	0.9918	0.8991 ± 0.0420	51.3095 ± 9.9844	60.7399 ± 25.4165
M7	3.6101	0.983	26.6595	0.993	69.3147	0.9909	0.9552 ± 0.2504	23.0232 ± 4.6367	69.2744 ± 31.2678
M8	3.5364	0.9884	40.7734	0.988	43.3217	0.9945	0.7966 ± 0.1435	28.2778 ± 2.5387	29.6404 ± 2.3163
M9	4.1259	0.989	40.7734	0.99	16.906	0.9948	1.1114 ± 0.3303	25.6856 ± 1.3749	8.9890 ± 0.8909
M10	3.5365	0.9897	33.007	0.988	53.319	0.9897	0.8142 ± 0.0309	22.2169 ± 2.1601	39.5042 ± 12.2305
M11	3.8723	0.9915	43.3217	0.988	43.3217	0.9703	0.7202 ± 0.0303	38.7184 ± 3.3964	41.0942 ± 10.5501
M12	3.1651	0.988	36.4814	0.989	40.7734	0.9898	0.5573 ± 0.0540	24.7642 ± 4.1252	70.7071 ± 18.2650
M13	5.3732	0.9885	31.5067	0.994	27.7259	0.997	0.6731 ± 0.04027	24.7642 ± 4.1252	70.5620 ± 58.4685
M14	4.1756	0.9865	43.3217	0.988	57.7623	0.9886	22.7715 ± 7. 1975	53.5537 ± 8.5492	41.3171 ± 18.3301
M15	3.9161	0.9895	40.7734	0.991	46.2098	0.9893	0.9687 ± 0.0615	60.5649 ± 18.1635	33.81457 ± 3.8399
M16	3.1796	0.9905	24.7553	0.992	53.319	0.9981	0.7902 ± 0.1375	30.0838 ± 2.7276	53.4001 ± 15.9178
M17	5.0967	0.9878	36.4814	0.992	99.021	0.9958	2.9738 ± 0.2184	56.2593 ± 9.3237	91.1618 ± 25.5012
M18	4.4719	0.9956	33.007	0.99	46.2098	0.9887	1.1200 ± 0.6280	36.9135 ± 6.9198	34.2783 ± 11.2224
M19	3.9161	0.982	31.5067	0.985	33.007	0.9957	0.6794 ± 0.0827	30.6040 ± 8.4389	27.2645 ± 11.7557
M20	3.7266	0.9818	53.319	0.989	38.5082	0.999	0.7159 ± 0.0411	45.2217 ± 0.2640	32.8195 ± 3.6766
Tacrine	15.065	0.9965	-	-	-	-	2.5860 ± 0.9000	-	-
Acetazolamide	-	-	46.2	0.992	38.5081	0.9914	-	36.3990 ± 9.0100	61.9282 ± 15.2536

Acetazolamide (AZA) was used as a standard inhibitor for both hCA I and II isoenzymes.

Tacrine (TAC) was used as a standard inhibitor for AChE isoenzyme.

* The CA inhibitory values of compounds **M1-M4** were taken from the previous study (Tugrak Sakarya et al. 2023).

results (Table 3), 4-fluoro-*N*-((4-sulfamoylphenyl)carbamothioyl)benzamide, compound **M1**, inhibited hCA I enzyme 2.2-fold more than compound **MD4** (4-fluoro-*N*-(4-oxo-3-(4-sulfamoylphenyl)thiazolidin-2-ylidene)benzamide), while compound **M9** (4-bromo-*N*-((4-sulfamoylphenyl)carbamothioyl)benzamide) inhibited 1.3-fold more than compound **MD3** (4-bromo-*N*-(4-oxo-3-(4-sulfamoylphenyl) thiazolidin-2-ylidene)benzamide). At the same time, **M13** (4-methoxy-N-((4-sulfamoylphenyl)carbamothioyl)benzamide) inhibited hCA I enzyme 1.8 times more than compound **MD1** (4-methoxy-*N*-(4-oxo-3-(4-sulfamoylphenyl) thiazolidin-2-ylidene)benzamide). Moreover, structure-activity relationship (SAR) investigations about the interactions between closely related enzymes and sulfonamides have resulted in valuable insights, demonstrating the concordance of findings through in vitro experimental assays and computational simulations (Table 3). Inhibition of hCA I within this compound series is highly sensitive to both steric and electronic factors surrounding the sulfonamide group, which serves as the primary pharmacophore. Accordingly, the chemical nature of the ring attached to the sulfonamide nitrogen plays a dominant role in modulating inhibitory potency. Compounds bearing an unsubstituted 4-sulfamoylphenyl moiety consistently exhibited stronger hCA I inhibition than their pyrimidinyl-substituted counterparts. Representative examples include **M1** (Ki = 19.88 ± 1.04 nM), **M5** (Ki = 24.0673 ± 1.9530 nM), **M9** (Ki = 25.6856 ± 1.3749 nM), and **M13** (Ki = 24.7642 ± 4.1252 nM). This trend suggests that the relatively planar and less sterically demanding phenyl ring allows optimal alignment of the sulfonamide in the active side. By contrast, pyrimidinyl substitution at the sulfonamide nitrogen generally reduced hCA I potency (such as **M2**, **M6**, and **M14**), most likely due to increased steric effects, altered electronic distribution, and unfavorable interactions that perturb the binding potency. The para-substitution pattern of the benzamide ring also influenced hCA I activity. Compounds bearing halogen substituents, particularly fluoro and chloro groups, tended to exhibit improved hCA I inhibition relative to strongly electron-donating or strongly electron-withdrawing groups. This behavior can be rationalized by a modest electronic tuning effect, whereby halogens subtly increase the acidity and binding efficiency of the sulfonamide. In contrast, nitro-substituted derivatives (**M17-M20**) generally showed weaker hCA I inhibition, likely because excessive electron withdrawal disturbs the delicate balance required for optimal binding potency.

For hCA isoenzyme, introduction of the thiazolidinone ring producedmoderate and substituent-dependent effects. The fluoro pair illustrates a slight weakening of activity: **M1** (Ki = 19.88 ± 1.04 nM) and **MD4** (Ki = 31.9922 ± 4.8999

nM). This suggests that cyclization slightly perturbs the optimal orientation of the sulfonamide in the active side. In the chloro series, the cyclization effect was not affected inhibition potency. **MD2** (Ki = 25.9595 ± 1.6014 nM) showed potency comparable to **M5** (Ki = 24.0673 ± 1.9530 nM). This may indicates that for chloro-substituted derivatives, the thiazolidinone ring does not significantly disrupt the positioning of the sulfonamide. For the bromo series, thiazolidinone conversion slightly decreased activity, **M9** (Ki = 25.6856 ± 1.3749 nM) and **MD3** (Ki = 33.9004 ± 2.5048 nM). In the methoxy series, hCA I inhibition was clearly weakened by cyclization: **M13** (Ki = 24.7642 ± 4.1252 nM) to **MD1** (Ki = 44.2911 ± 5.7516 nM), indicating that electron-donating groups in combination with a rigid scaffold are less compatible with hCA I active site constraints.

As a result, the thiazolidinone scaffold generally reduces hCA I inhibitory potency, although modest improvements or neutral effects can occur depending on substituent electronics. hCA I appears highly sensitive to subtle geometric changes around the sulfonamide group.

Cytosolic hCA II isoform was inhibited by many thiourea-substituted benzenesulfonamides **M1-M20** with varying degrees of potency. All the synthesized compounds were potent hCA II inhibitors with Ki values ranging between 8.15 ± 1.50 nM and 91.1618 ± 25.5012 nM. They acted as strong inhibitors except compounds of **M7**, **M12**, **M13**, and **M17** compared with AZA (Ki of 61.9282 ± 15.2536 nM). Compound **M9**, with a Ki of 8.9890 ± 0.8909 nM and compound **M3** with a Ki of 8.15 ± 1.50 nM (Table 1), were the compounds with the highest potency among the derivatives, whereas compound **M17**, with a Ki value of 91.1618 ± 25.5012 nM, was the least potent inhibitor of hCA II. Compound **M9** appears to be the most effective compound in the series because it shows strong inhibition at the lowest concentration in terms of both IC_{50} value and Ki value. The inhibitory activities of the thiourea-substituted benzenesulfonamides against hCA II followed the decreasing order of **M9** ~ **M3** > **M2** > **M1** > **M19** > **M8** > **M5** > **M20** > **M15** > **M18** > **M10** > **M11** > **M14** > **M4** > **M16** > **M6** > **M7** > **M13** > **M12** > **M17** (Table 1).

Based on the Ki values, compounds **MD1-MD4** strongly inhibited hCA II isoenzyme, with Ki values of 27.234 ± 1.9478 to 40.6423 ± 5.8751 nM, whereas AZA's Ki value was 61.9282 ± 15.2536 nM against hCA II isoenzyme. Thus, the hCA II isoenzyme inhibition potency of the compounds was 2.3 – 1.5 times more than AZA. Compound **MD2** (4-chloro-*N*-(4-oxo-3-(4-sulfamoylphenyl)thiazolidin-2-ylidene)benzamide) can be considered as a promising inhibitor against hCA II isoenzyme in the series, with Ki = 27.234 ± 1.9478 nM (Table 3).

In contrast to hCA I, the inhibition profile of hCA II reveals a distinct sensitivity to lipophilic and steric modifications, reflecting structural differences in the active site architecture and the availability of secondary hydrophobic pockets. Unlike the trend observed for hCA I, pyrimidinyl at the sulfonamide nitrogen proved to be advantageous for hCA II inhibition. The most potent compound in this series, **M3** (4-fluoro benzamide bearing a 4-methylpyrimidin-2-yl sulfonamide; Ki = 8.15 ± 1.50 nM) exemplifies this effect. The presence of a small methyl group on the pyrimidine ring likely enhances local lipophilicity and shape complementarity, facilitating improved packing within a hydrophobic pocket. Unsubstituted phenyl sulfonamides also demonstrated strong hCA II inhibition when combined with suitable benzamide substituents. For example, **M9** (4-bromo benzamide with an unsubstituted sulfonamide phenyl ring) showed potent activity (Ki = 8.9890 ± 0.8909 nM), indicating that both optimized hydrophobic pocket occupation and geometry can independently drive high hCA II affinity. The nature of the para-substituent on the benzamide ring further influenced hCA II potency. Larger, more polarizable halogens such as bromine tended to enhance activity, likely through reinforced hydrophobic and dispersion interactions with hCA II-specific surface features. In contrast, methoxy and nitro-substituted derivatives generally failed to provide systematic improvements in hCA II inhibition, with their effects being highly dependent on the identity of the sulfonamide-bound ring. In summary, hCA II inhibition appears to benefit from the introduction of small lipophilic substituents on heteroaromatic sulfonamide moieties and/or bulky, polarizable halogens on the benzamide ring.

In the fluoro series, hCA II affinity improved upon thiazolidinone formation: **M1** (Ki = 49.86 ± 6.18 nM) and **MD4** (Ki = 40.6423 ± 5.8751 nM). Although the improvement was modest, it suggests that hCA II can better accommodate the more rigid binding geometry. A clear enhancement was observed for the methoxy-substituted compounds, where **MD1** (Ki = 31.7732 ± 4.2135 nM) was substantially more potent than **M13** (Ki = 70.5620 ± 58.4685 nM). This situation may indicate that the thiazolidinedione ring contributes to interactions in the active site in hCA II inhibition. While the **M5** → **MD2** conversion resulted in a slight improvement in hCA II inhibitory activity (32.4192 ± 7.1743 → 27.234 ± 1.9478 nM), the **M9** → **MD3** conversion caused a marked loss of potency (8.9890 ± 0.8909 → 32.9767 ± 2.6001 nM). The strong potency of **M9** was not preserved in **MD3**, implying that hCA II strongly favors the particular geometry provided by the open-chain benzamide scaffold in the presence of a bromo substituent.

AChE inhibitory effects

The present work represents a continuation of our previously published studies (Tugrak et al. 2021c; Tugrak

Sakarya et al. 2023) where related acylthiourea and sulfonamide-based derivatives demonstrated promising inhibitory activity against the same therapeutic enzyme classes. Based on these prior findings, we deliberately selected the benzenesulfonamide core and merged it with thiourea and thiazolidinone frameworks to further optimize potency and multi-target potential (Tugrak Sakarya et al. 2023).

Given that thiourea/acylthiourea derivatives exhibit potential in relation to Alzheimer's, these compounds were examined as AChE inhibitors. All of the synthesized compounds **M1-M20** were screened for their in vitro inhibitory activity against AChE (from Electrophorus electricus) using the modified Ellman's method (Ellman et al. 1961). Reference drugs' Ki values were the average of three independent experimental values. The obtained results are presented in Table 1. Overall, compounds **M1-M20** showed stronger inhibitory activity against AChE than tacrine (except **M14**, **M17**). In the case of AChE, halogen groups markedly affected the inhibitory activity. Thioureas **M14** and **M17** showed the weakest inhibition against AChE (with Ki > 2.5 nM). However, the remaining compounds showed quite strong inhibitory activity, with Ki < 2 nM, comparable to tacrine. Among the compounds with potential activity, thiourea **M1** showed stronger inhibition than the comparable drug compound, with a Ki value of 2.5860 ± 0.9000 nM of tacrine. Thioureas **M1** (0.4740 ± 0.0818 nM) showed 6.2-fold more activity than compound Tacrine. The AChE inhibitory activity of these potential compounds in descending order was as follows: **M1** > **M12** > **M4** > **M2** > **M13** > **M19** > **M20** > **M11** > **M16** > **M8** > **M3** > **M10** > **M6** > **M7** > **M15** > **M5** > **M9** > **M18** > **M17** > **M14**. The newly synthesized thiazolidinone derivatives (**MD1-MD4**) were alsoscreened for their anti-cholinesterase activity using tacrine as a standard reference. The Ki values for AChE inhibition are shown in Table 3. The results presented in the table suggest that most of the tested compounds exhibit moderate to good inhibitory activities in the low micromolar range. Compound **MD1** was the most potent one with a Ki value of 0.6731 ± 0.04027 nM, and it has a 4-methoxy substituent on the phenyl ring. Interestingly, the replacement of the chloro group at the same position on the phenyl ring in compound **MD2** resulted in a noticeable loss of activity as it had a Ki value of 2.9412 ± 0.2323 nM. The inhibitory potency of the compound **MD3** reflected that the bromo group substituent in the core of the molecule is of great value in terms of its potency. It has a Ki value of 2.2725 ± 0.2112 nM. Fluoro-substituted compound **MD4** showed a Ki value of 2.4872 ± 0.3026 nM.

The AChE inhibition profile of the series is characterized by very high potency across most derivatives, with Ki values predominantly in the low-nanomolar to sub-nanomolar range. The observed activity is mainly controlled by two structural factors: (i) the nature of the para-substituent on the benzamide phenyl ring and (ii) the chemical identity of the ring attached to the sulfonamide nitrogen. Halogenated derivatives (F, Cl, and Br) consistently exhibited the strongest AChE inhibition. In particular, the 4-fluoro analogue (**M1**, Ki = 0.4740 ± 0.0818 nM) emerged as one of the most potent compounds, while 4-chloro and 4-bromo analogues (**M5** and **M9**) and their pyrimidinyl counterparts retained similarly high activity. This behavior may be rationalized by enhanced hydrophobic and π–π interactions within the aromatic gorge of AChE, as well as potential halogen-dependent interactions with amino acid residues.

Electron-donating substituents such as methoxy groups were generally well tolerated; however, their effect was context-dependent. While some 4-methoxy derivatives (**M13, Ki=0.6731 ± 0.04027 nM**) preserved strong activity, the combination of the methoxy group with heteroaromatic sulfonamides (as in **M14**, Ki = 22.7715 ± 7.1975 nM) led to a marked reduction in potency. This suggests that excessive electronic donation and steric demand may disrupt the optimal binding orientation within the active site.

Compounds bearing an unsubstituted 4-sulfamoylphenyl moiety at the sulfonamide nitrogen generally showed superior AChE inhibitory activity. The planar nature of the phenyl ring likely facilitates favorable alignment of the scaffold, enabling efficient penetration into the enzyme. In contrast, pyrimidinyl-substituted analogues maintained high activity in most cases, with the impact on potency depending on the substitution pattern of the heteroaromatic ring. Notably, the introduction of small lipophilic groups on the pyrimidine ring (a 4-methyl group in **M3**) did not compromise activity and frequently preserved sub-nanomolar inhibition.

In summary, the data indicate that halogen substitution on the benzamide ring, particularly fluorine and bromine, combined with a relatively planar sulfonamide-attached aromatic system, provides the most favorable structural features for potent AChE inhibition. Avoidance of strongly electron-donating para-substituents in conjunction with bulky heteroaromatic sulfonamide groups appears to be critical for maintaining maximal inhibitory potency.

The conversion of the flexible benzamide-thiourea scaffold (M-series) into the more conformationally constrained thiazolidinone framework (MD-series) resulted in divergent effects on AChE inhibition that strongly depend on the nature of the para-substituent on the benzamide ring. For the fluoro-substituted pair, the parent compound **M1** (Ki = 0.4740 ± 0.0818 nM) exhibited extremely potent inhibition, whereas its thiazolidinone analogue **MD4** showed a marked loss of activity (Ki = 2.4872 ± 0.3026 nM). Although **MD4** remained within the low-nanomolar range, the decrease indicates that rigidification of the scaffold may partially disrupt the optimal alignment within the AChE active site, which appears to favor the more flexible

benzamide–thiourea motif in this case. A more dramatic loss of activity was observed for the chloro-substituted pair. While **M5** (Ki = 1.0147 ± 0.1725 nM) was highly potent, its thiazolidinone derivative **MD2** showed a substantial drop in potency (Ki = 2.9412 ± 0.2323 nM). This may suggest that for chloro analogues, thiazolidinone ring closure imposes a suboptimal geometry, likely preventing efficient simultaneous engagement of the active sites. For the bromo series, the parent compound **M9** (Ki = 1.1114 ± 0.3303 nM) was highly active, whereas **MD3** lost potency (Ki = 2.2725 ± 0.2112 nM) but still retained low-nanomolar inhibition. This indicates that the bromo group is more tolerant to conformational restriction, possibly due to favorable hydrophobic and polarizability-driven interactions that partially compensate for geometric changes. In contrast, in the methoxy-substituted series, the thiazolidinone transformation had a similar effect. **M13** (Ki = 0.6731 ± 0.04027 nM) and **MD1** (Ki = 0.6731 ± 0.04027 nM) displayed nearly identical potency. This suggests that electron-donating substituents may better option the change in geometry, possibly through alternative hydrogen-bonding or dipolar stabilization inside the AChE binding site.

As a result, cyclization into the thiazolidinone core generally reduces AChE affinity relative to the parent benzamide scaffold, with the exception of methoxy-substituted systems. The data support the idea that AChE strongly favors a flexible, extended conformation, while rigidified analogues suffer from partial misalignment unless electronic factors compensate.

α-Glucosidase activity and α-Amylase activity

Currently, oral α-glycosidase inhibitors like miglitol, acarbose, and vembibose are routinely used to reduce blood sugar levels. These drugs are unique in that they do not address the pathophysiology of T2DM. These chemicals have good safety qualities and do not cause hypoglycemia. However, gastrointestinal side effects may restrict long-term therapy compliance (Hayat et al. 2023; Iqbal et al. 2025; Ch'ng et al. 2019; Saltos et al. 2015; Taslimi et al. 2018). Therefore α-glycosidase and α-amylase enzyme inhibitory activities of the compounds were evaluated.

For the α-glycosidase enzyme, the novel thiourea derivatives (**M1-M20**) had Ki values in the range of 4.9395 ± 0.8288 – 46.1207 ± 19.5197 nM (Table 2). The results clearly recorded that all thiourea derivatives (**M1-M20**) demonstrated efficient α-glycosidase inhibitory effects than that of acarbose's Ki= 48.52 ± 8.08 nM as a standard α-glycosidase inhibitor. Indeed, the most effective Ki values were obtained by **M10** and **M8** with Ki values of 4.9395 ± 0.8288 nM and 6.0786 ± 0.5732 nM, respectively. Ki values of compounds **MD1-MD4** were also in the range of 10.5176 ± 3.0458 nM to 37.3676 ± 7.71632 nM on α-glycosidase, whereas Acarbose's Ki values were 48.52 ± 8.08 nM. Compound **MD2**, 4-chloro-*N*-(4-oxo-3-(4-sulfamoylphenyl)thiazolidin-2-ylidene)benzamide, was the best inhibitor against α-glycosidase with 10.5176 ± 3.0458 nM (Table 3).

The α-glucosidase inhibitory profile of the synthesized thiourea-sulfonamide derivatives revealed a pronounced dependence on both the para-substituent of the

Table 2 α-Glycosidase and α-amylase inhibitory activities of thiourea-based sulfonamide derivatives (**M1-M20**)

Compounds	IC_{50} (nM)			Ki (nM)	
	α-glycosidase	r^2	α-amylase	r^2	α-glycosidase
M 1	22.3596	0.9904	21.290	0.9904	10.7113 ± 1.2290
M 2	15.0684	0.9906	16.056	0.9924	8.8654 ± 1.9117
M 3	12.6027	0.9914	16.275	0.9899	12.4072 ± 0.2767
M 4	8.3512	0.9899	16.637	0.9944	6.2425 ± 3.2858
M 5	25.6721	0.9921	14.936	0.9793	9.9056 ± 1.9365
M 6	57.7623	0.9904	15.651	0.9905	27.4624 ± 2.6947
M 7	18.2407	0.9911	17.543	0.9898	14.6551 ± 2.0794
M 8	11.1798	0.9905	15.956	0.9944	6.0786 ± 0.5732
M 9	9.627	0.9823	19.473	0.999	7.5800 ± 0.5665
M 10	8.1546	0.9908	19.354	0.9936	4.9395 ± 0.8288
M 11	33.007	0.9925	26.124	0.9697	18.8481 ± 3.6804
M 12	25.6721	0.9973	20.187	0.8761	24.4036 ± 9.2247
M 13	38.5082	0.9915	56.533	0.983	30.6510 ± 8.2385
M 14	38.5082	0.9877	17.472	0.9644	9.8245 ± 2.7028
M 15	17.773	0.9923	13.47	0.9576	16.0002 ± 3.9400
M 16	23.1049	0.9923	13.164	0.9594	13.8855 ± 6.1975
M 17	69.3147	0.9869	12.044	0.9621	29.1161 ± 15.3029
M 18	24.7553	0.9951	12.845	0.9715	17.1707 ± 6.6380
M 19	46.2098	0.9906	13.011	0.9988	42.2915 ± 15.3339
M 20	46.2098	0.9888	18.089	0.9802	46.1207 ± 19.5197
Acarbose	51.45	0.9981	15.92	0.9904	48.52 ± 8.08

Acarbose (ACR) was used as a standard inhibitor for α-glycosidase and α-amylase enzymes.

Table 3 Enzyme inhibitor activities of thiazolidinone derivatives **MD1-MD4**

	IC_{50} (nM)							Ki (nM)				
Compounds	AChE	r^2	hCA I	r^2	hCA II	r^2	α-glycosidase	r^2	α-amylase	r^2	AChE	hCA I	hCA II	α-glycosidase
MD 1	4.2524	0.9865	53.319	0.991	34.6574	0.9884	46.2098	0.9832	34.2469	0.994	0.6731 ± 0.04027	44.2911 ± 5.7516	31.7732 ± 4.2135	37.3676 ± 7.71632
MD 2	4.7476	0.9922	53.319	0.986	26.6595	0.9981	17.3287	0.9914	15.929	0.999	2.9412 ± 0.2323	25.9595 ± 1.6014	27.234 ± 1.9478	10.5176 ± 3.0458
MD 3	4.4433	0.9926	38.5082	0.989	38.5082	0.9942	27.7259	0.9911	15.929	0.999	2.2725 ± 0.2112	33.9004 ± 2.5048	32.9767 ± 2.6001	20.8903 ± 3.2419
MD 4	4.6209	0.9904	46.2098	0.993	43.3217	0.9932	34.6573	0.9904	17.882	0.998	2.4872 ± 0.3026	31.9922 ± 4.8999	40.6423 ± 5.8751	12.7068 ± 3.4426
Tacrine	15.065	0.9965	–	–	–	–	–	–	–	–	2.5860 ± 0.9000	–	–	–
Asetazolamide	–	–	46.2	0.992	38.5081	0.9914	–	–	–	–	–	36.3990 ± 9.0100	61.9282 ± 15.2536	–
Acarbose	–	–	–	–	–	–	51.45	0.9981	15.92	0.9904	–	–	–	48.52 ± 8.08

benzamide ring and the heteroaromatic character of the sulfonamide-bound moiety. Compounds bearing a 4-fluoro benzamide group displayed the most consistent and potent α-glucosidase inhibition. In particular, the introduction of alkyl-substituted pyrimidinyl rings significantly enhanced activity. The dimethyl-substituted pyrimidine analogue **M4** ($IC_{50} \approx 8.35$ nM) emerged as the most potent inhibitor in this series, indicating that increased lipophilicity and steric bulk at the pyrimidine ring promote productive interactions with the enzyme binding pocket.

A clear activity trend within the fluoro series was observed: Dimethylpyrimidinyl **(M4)** > 4-methylpyrimidinyl (**M3**) > pyrimidinyl (**M2**) > unsubstituted phenyl (**M1**), suggesting that gradual hydrophobic reinforcement around the sulfonamide nitrogen enhances α-glucosidase affinity. Chloro-substituted derivatives showed a more variable activity profile. While the dimethyl-pyrimidinyl compound **M8** ($IC_{50} \approx 11.18$ nM) retained good potency, the parent pyrimidinyl compound **M6** ($IC_{50} \approx 57.76$ nM) suffered a marked loss of activity, implying that excessive polarity orunfavorable orientation of the heteroaromatic ring may be detrimental unless compensated by hydrophobic substituents. Bromo-substituted analogues **M9** (phenyl, $IC_{50} \approx 9.63$ nM) and **M10** (pyrimidinyl, $IC_{50} \approx 8.15$ nM) showed strong inhibition, indicating that larger, more polarizable halogens may favor hydrophobic and dispersion-type interactions within the α-glucosidase active site. Conversely, electron-donating (methoxy) and strongly electron-withdrawing (nitro) substitutions were less favorable. Methoxy derivatives (**M13**-**M16**) and nitro derivatives (**M17**-**M20**) generally exhibited reduced α-glucosidase inhibition, with significantly higher IC_{50} values. This suggests that extreme electronic perturbation of the benzamide ring disrupts optimal enzyme-ligand complementarity. Overall, α-glucosidase inhibition was maximized by the combination of halogenated benzamide rings (F, Br) and hydrophobically substituted pyrimidinyl sulfonamides, supporting a model in which both lipophilicity and steric occupancy of the binding pocket are critical determinants of activity.

For α-glucosidase enzyme, thiazolidinone formation generally led to retention or improvement of potency. The most striking gain was seen for the chloro derivative, where **MD2** (Ki = 10.5176 ± 3.0458 nM) was dramatically more potent than the corresponding parent series compound **M5**. The fluoro analogue **MD4** (Ki = 12.7068 ± 3.4426 nM) and the bromo analogue **MD3** (Ki = 20.8903 ± 3.2419 nM) also showed strong activity, exceeding the reference compound acarbose (Ki = 48.52 ± 8.08 nM). Thiazolidinone ring formation substantially benefits α-glucosidase inhibition, indicating that this enzyme favors a more compact, preorganized ligand geometry.

All the compounds (**M1-M20**) showed α-amylase inhibitory potential with IC_{50} ranging from 12.044 to 56.533 nM as compared to standard drugs Acarbose (IC_{50} = 15.92 nM) (Table 2). Compound **M17** is the most potent, while compound **M13** is the least potent among the series. Compound **M17** (IC_{50} = 12.044 nM) contains a nitro group at the para position of the phenyl ring and is the most potent among the series. The greater potency of this compound might be due to the presence of the nitro group, which might be involved in hydrogen bonding. If we compare compound **M17** (IC_{50} = 12.044 nM), which also contains a nitro group at the para position on one phenyl ring, with compound **M1** (IC_{50} = 21.290 nM), in which the nonsubstituted phenyl ring, compound **M17** is more potent than compound **M1**. This may be due to the effects of the nitro group on the phenyl ring. IC_{50} values of some thiourea derivatives (**M1-M20**) on α-amylase enzyme exhibited the following order: **M17** (IC_{50}= 12.044 nM) > **M18** (IC_{50}= 12.845 nM) > **M19** (IC_{50}= 13.011 nM) > **M16** (IC_{50}= 13.164 nM) > **M15** (IC_{50}= 13.47 nM) > **M5** (IC_{50}= 14.936 nM) > **M6** (IC_{50}= 15.651 nM) > **M8** (IC_{50}= 15.956 nM) > **M2** (IC_{50}= 16.056 nM) > **M3** (IC_{50}= 16.275 nM) > **M4** (IC_{50}= 16.637 nM) > **M14** (IC_{50}= 17.472 nM) > **M7** (IC_{50}= 17.543 nM) > **M20** (IC_{50}= 18.089 nM) > **M10** (IC_{50}= 19.354 nM) > **M9** (IC_{50}= 19.473 nM) > **M12** (IC_{50}= 20.187 nM) > **M1** (IC_{50}= 21.290 nM) > **M11** (IC_{50}= 26.124 nM) > **M13** (IC_{50}= 56.533 nM) (Table 2).

In contrast to α-glucosidase, the α-amylase inhibition data indicated a distinct structure-activity trend, suggesting fundamentally different recognition requirements between the two carbohydrate-processing enzymes. The most potent α-amylase inhibitors were predominantly found among compounds bearing electron-donating or strongly electron-withdrawing substituents, particularly when combined with heteroaromatic sulfonamide fragments. Notably, the nitro-substituted derivatives such as **M17** (IC_{50}= 12.044 nM) and **M18** (IC_{50}= 12.845 nM) exhibited superior potency relative to many halogenated analogues, highlighting a preference of α-amylase for highly polarized or hydrogen-bond-enriched ligands. Within the methoxy-substituted series, compounds **M15** (IC_{50}= 13.47 nM) and **M16** (IC_{50}= 13.16 nM) showed strong inhibition, indicating that electron-donating oxygenated substituents enhance affinity, possibly *via* additional hydrogen-bonding or dipolar interactions with catalytic residues. Halogenated compounds showed moderate activity. Fluoro- and chloro-substituted derivatives presented IC_{50} values around 15–21 nM, suggesting that hydrophobic or dispersion-driven interactions are less dominant in α-amylase than in α-glucosidase binding. Interestingly, bulky or highly hydrophobic combinations led to reduced α-amylase potency. Compared with the reference inhibitor acarbose (IC_{50}= 15.92 nM), several compounds (**M15-M18**) demonstrated comparable or superior potency, underscoring the potential of this scaffold as a dual α-amylase/α-glucosidase inhibitor.

The inhibitory profiles of **MD1-MD4** molecules were found to be different from each other due to different substituents in the para position. Compound **MD2** contains one chlorine group at the para position, while compound **MD3** contains a bromo group at the para position showed the same inhibitory effects in α-amylase with IC_{50} = 15.929 nM. In case of compound **MD1**was found with somewhat lower activity in α-amylase (IC_{50} = 34.2469 nM) than standard acarbose (IC_{50} = 15.92 nM). In the series, compound **MD2** showed the strongest inhibitory property against α-amylase and α-glucosidase while **MD1** showed the lowest inhibitory effect (Table 3).

The integration of thiazolidinone and thiourea/acylthiourea pharmacophores with the benzenesulfonamide core appears to contribute to improved inhibitory potency. The enhanced activities observed for selected compounds can be attributed to the synergistic effects of multiple interaction-capable functional groups, enabling hydrogen bonding, hydrophobic, π–π stacking, and potential interactions within enzyme active sites. These bioactivity findings suggest that the pharmacophore hybridization approach represents a useful design principle for the development of multi-target enzyme inhibitors and may guide the future optimization of related molecular frameworks.

Molecular docking

A computer method called molecular docking is used to forecast a ligand's preferred orientation and binding affinity when it interacts with a target protein. Docking helps identify possible inhibitors for therapeutic targets and offers vital insights into the mechanics of binding by mimicking these chemical interactions. Because it makes it possible to quickly and affordably screen vast libraries of chemicals, this technique is essential to contemporary drug development as it helps to identify potential candidates for experimental validation. Moreover, molecular docking improves knowledge of structure-activity connections, which makes it easier to create molecules that are more selective and effective. It is a vital tool in medicinal chemistry, helping to develop tailored treatments for a variety of ailments because of its capacity to mimic intricate molecular interactions (Taylor et al. 2002; Ferreira et al. 2015; Meng et al. 2011). Based on experimental data, the **M1** molecule demonstrated effective inhibition of the hCAI and AChE receptors, while the **M9** molecule exhibited inhibition of the hCAII receptor. Additionally, the **M10** molecule successfully inhibited the α-glucosidase receptor, and the **M17** molecule showed inhibitory activity against the α-amylase receptor. At this stage of the study, we aimed to corroborate these inhibitory interactions through

in-silico analyses alongside the experimental results. Consequently, theoretical calculations were conducted for these four precursor compounds (**M1**, **M9**, **M10**, and **M17**) out of the 24 molecules in the series. The calculations for molecular docking were completed with the Autodock Vina programme (Trott and Olson 2010). The PDB structures used for the ligand molecules were obtained from the theoretical optimizations. The Discovery Studio Visualizer 4.0 (DSV 4.0) program was used for all ligand-related procedures, including the conversion of the ligands (**M1**, **M9**, **M10**, and **M17**) into PDB and PDBQT formats (Scientific Software http://www.3dsbiovia.com/). The target proteins chosen for this investigation were hCAI (PDB ID: 2CAB) (Kannan et al. 1984; Mahmudov et al. 2022), AChE (PDB ID: 1EVE) (Mahmudov et al. 2022; Kryger et al. 1999), hCAII (PDB ID: 5AML) (Mahmudov et al. 2022; Ivanova et al. 2015), α-glucosidase (PDB: 3A4A) (Chen et al. 2023; Protein data Bank et al. 2000 https://www.rcsb.org/.) and α-amylase (PDB: 1SMD) (Protein data Bank et al. 2000 https://www.rcsb.org/.; Saleh 2024) receptors in accordance with experimental procedures and pertinent literature. The RCSB Protein Data Bank (PDB) provided the three-dimensional PDB structures of these receptors (Protein data Bank. https://www.rcsb.org/.). Heteroatoms found in the five target proteins were also eliminated with Discovery Studio Visualizer 4.0 (DSV 4.0) (Scientific Software http://www.3dsbiovia.com/). After adding polar hydrogen atoms and the associated charges, the processed data was once more recorded in PDB and PDBQT formats. The following critical residues and active sites of the target proteins were found to improve the accuracy of the docking analysis: HIS119, HIS96, HIS94 for hCAI (PDB ID: 2CAB); HIS440, PHE330, GLU327, TRP279, SER200, TRP84 for AChE (PDB ID: 1EVE; THR200, THR199, LEU198, PHE131, VAL121, HIS119, HIS96, HIS94, GLN92, ASN67, and ASN62 for hCAII (PDB ID: 5AML); ARG337, ASN298, HIS201, ARG195, ASP167, AG158, ASN100 for α-amylase (PDB ID: 1SMD) (Mert et al. 2025). The grid parameters listed below were created to account for these active zones: $40 \times 40 \times 40$ Å^3 x, y, z dimensions, 0.375 Å space and 39.041, -10.534, 10.394 x, y, z centers for hCAI/PDB: 2CAB; $44 \times 44 \times 38$ Å^3 x, y, z dimensions, 0.375 Å space and −0.39, 63.448, 67.71 x, y, z centers for AChE/PDB: 1EVE; $32 \times 40 \times 32$ Å^3 x, y, z dimensions, 0.375 Å space and −5.915, 5.359, 16.391 x, y, z centers for hCAII /PDB: 5AML; and $40 \times 40 \times 40$ Å^3 x, y, z dimensions, 0.375 Å space and 8.343, 58.71, 19.126 x, y, z centers for α-amylase/PDB: 1SMD (Khan et al. 2022). Since active residues for the α-glucosidase target could not be found in the literature, the grid parameters were taken as follows, according to the region with the highest binding energy: $40 \times 40 \times 40$ Å^3 x, y,z dimensions, 0.375 Å space, and 21.272, -0.751, 18.633 x, y, z centers for α-glucosidase/PDB: 3A4A. Molecular docking results for **M1**, **M9**, **M10**, and **M17** ligands and interactions with related proteins are given in Table 4.

Table 4 Molecular docking scores of **M1**, **M9**, **M10** and **M17** compounds

Compounds	hCA I/PDB: 2CAB+M1 ligand	AChE/PDB: 1EVE+M1 ligand
M1	E=-10.5 kcal/mol Hidrogen bond numbers = 5 Ki = 20.1115 nM	E=-12.6 kcal/mol Hidrogen bond numbers = 4 Ki = 0.580942 nM
M9	**hCA II/PDB: 5AML+M9 ligand** E=-11.0 kcal/mol Hidrogen bond numbers = 5 Ki = 8.64851 nM	
M10	**α-glucosidase/PDB: 3A4A+M10 ligand** E=-11.6 kcal/mol Hidrogen bond numbers = 5 Ki = 3.14151 nM	
M17	**α-amylase/PDB: 1SMD+M17 ligand** E=-11.1 kcal/mol Hidrogen bond numbers = 2 Ki = 7.30535 nM	

In addition, Table 4 shows the values of Ki, i.e. inhibition constant, calculated based on the conventional hydrogen bond numbers and binding energies formed in the interactions of molecules with proteins. Utilizing the Ki = exp(-G/RT) equation, the inhibition values for **M1**, **M9**, **M10**, and **M17** + related proteins were calculated ("G-binding energy, R-gas constant = 1.9872036×10^{-3} kcal/mol, and T-temperature = 298.15 K"). In these interactions, the positions of the molecules in the active sites of the proteins and the 3D and 2D forms of the interactions are presented in Figs. 3, 4, 5, 6, 7, 8, 9, 10 for **M1**, **M9**, **M10**, and **M17** molecules, respectively.

Figures 3, 4, 5, 6, 7, 8, 9, and 10 offer detailed visualizations of the molecular docking interactions for **M1**, **M9**, **M10**, and **M17** with their corresponding protein targets: hCAI, AChE, hCAII, α-glucosidase, and α-amylase. The 3D and 2D depictions display the exact positioning of these molecules within the active sites, showcasing critical interactions such as hydrogen bonds and binding affinities. **M1** exhibited significant binding to hCAI (PDB: 2CAB) and AChE (PDB: 1EVE), whereas **M9** displayed notable affinity for hCAII (PDB: 5AML). **M10** and **M17** showed effective interactions with α-glucosidase (PDB: 3A4A) and α-amylase (PDB: 1SMD), respectively. The binding energy values and predicted inhibition constants (*Ki*) support the effectiveness of these molecules, aligning closely with experimental findings. These results highlight the robustness of the computational approach in identifying potential

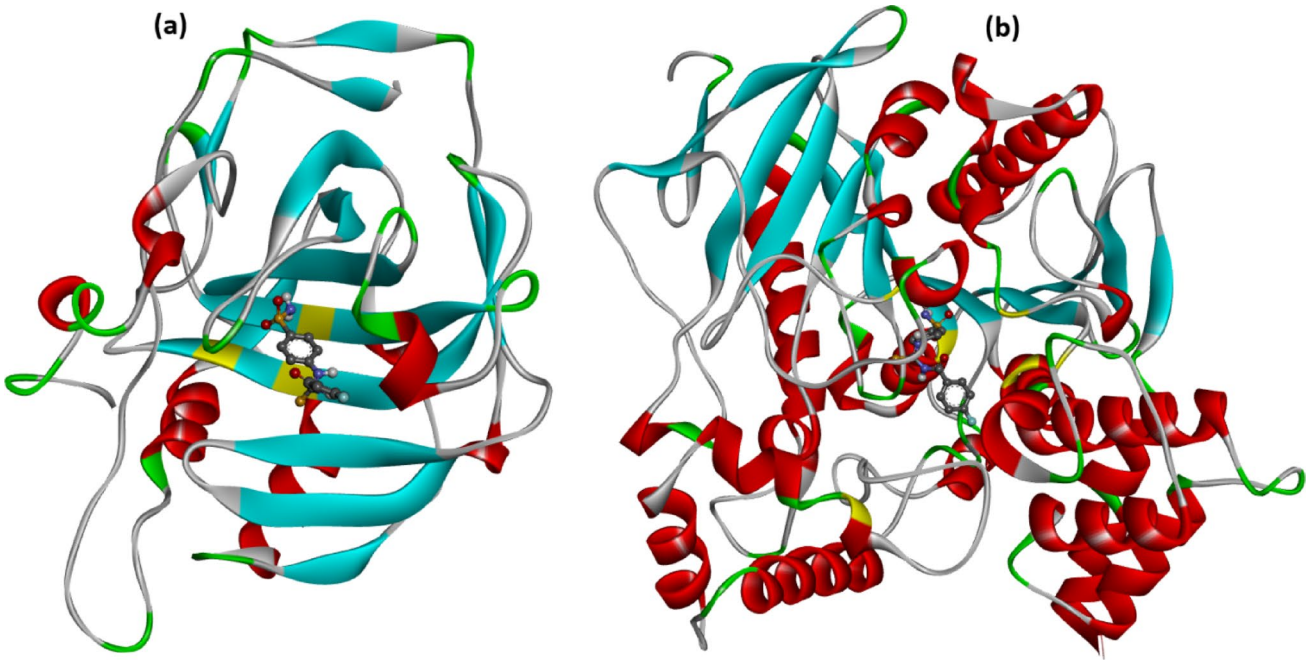


Fig. 3 The localization of the molecule **M1** to the active sites of the proteins 2CAB (**a**) and 1EVE (**b**)

inhibitors and provide critical insights into the structure-activity relationships, aiding future drug development and therapeutic research.

.

As shown in Fig. 4b, the **M1**–hCA I (PDB: 2CAB) complex is stabilized by five hydrogen bonds, involving THR199-O (3.05 and 3.12 Å), HIS94-H (2.97 Å), HIS119-O (2.09 Å), and GLN92-S (3.75 Å). These interactions include catalytically important residues and indicate a favorable accommodation of **M1** within the hCA I active site. Likewise, the **M1**–AChE (PDB: 1EVE) interaction depicted in Fig. 4d reveals four hydrogen bonds with GLY118-O (3.14 Å), GLU199-H (2.32 Å), TYR130-H (2.66 Å), and TYR121-H (2.10 Å), all located within the catalytic gorge, supporting the strong experimental AChE inhibition of **M1**. For compound **M9**, docking analysis in Fig. 6b shows the formation of six hydrogen bonds with hCA II (PDB: 5AML), including interactions with GLN92-O (4.21 Å), THR199-O (3.32 Å), THR199-H (3.06 Å), HIS96-H (5.52 Å), HIS94-S (5.23 Å), and HIS119-O (3.82 Å). The involvement of zinc-associated residues HIS94, HIS96, and HIS119 highlights direct interaction with the catalytic core, explaining the high inhibitory potency of **M9**. As illustrated in Fig. 8b, M10 forms five hydrogen bonds within the α-glucosidase (PDB: 3A4A) active site, involving SER241-Br (3.70 Å), TYR158-H (3.80 Å), ASN415-S (5.86 Å), GLN279-O (5.71 Å), and ARG442-N (6.33 Å). Despite relatively longer interaction distances, the combined hydrogen-bonding and electrostatic contributions appear sufficient to stabilize **M10** in the binding pocket. Finally, docking of **M17** with α-amylase (PDB: 1SMD) shown in Fig. 10b reveals two key hydrogen bonds with HIS305-H (2.67 Å) and SER163-S (3.32 Å). Although fewer in number, these interactions involve catalytically relevant residues and are consistent with the strong α-amylase inhibitory activity observed experimentally.

Validation of the docking protocol

Although redocking of co-crystallized ligands was not performed, the docking workflow follows the standard AutoDock Vina parameters that have been widely validated to reproduce experimental ligand poses with acceptable RMSD values. The grid settings and search parameters used here are consistent with those reported in previous Vina benchmarks. The predicted interactions also agree with the known structural features of the enzyme active sites, supporting the reliability of the docking approach.

Relation of docking predictions to experimental inhibition trends

The docking results for **M1**, **M9**, **M10** and **M17** show a clear qualitative correspondence with their experimental inhibitory profiles. The strongest inhibitors identified in vitro (**M1** for AChE and hCA I, **M9** for hCA II, **M10** for α-glucosidase, and **M17** for α-amylase) also ranked among the top-scoring ligands in the docking simulations, exhibiting lower binding energies and multiple stabilizing hydrogen bonds within the active sites. Conversely, compounds with weaker experimental inhibition displayed less

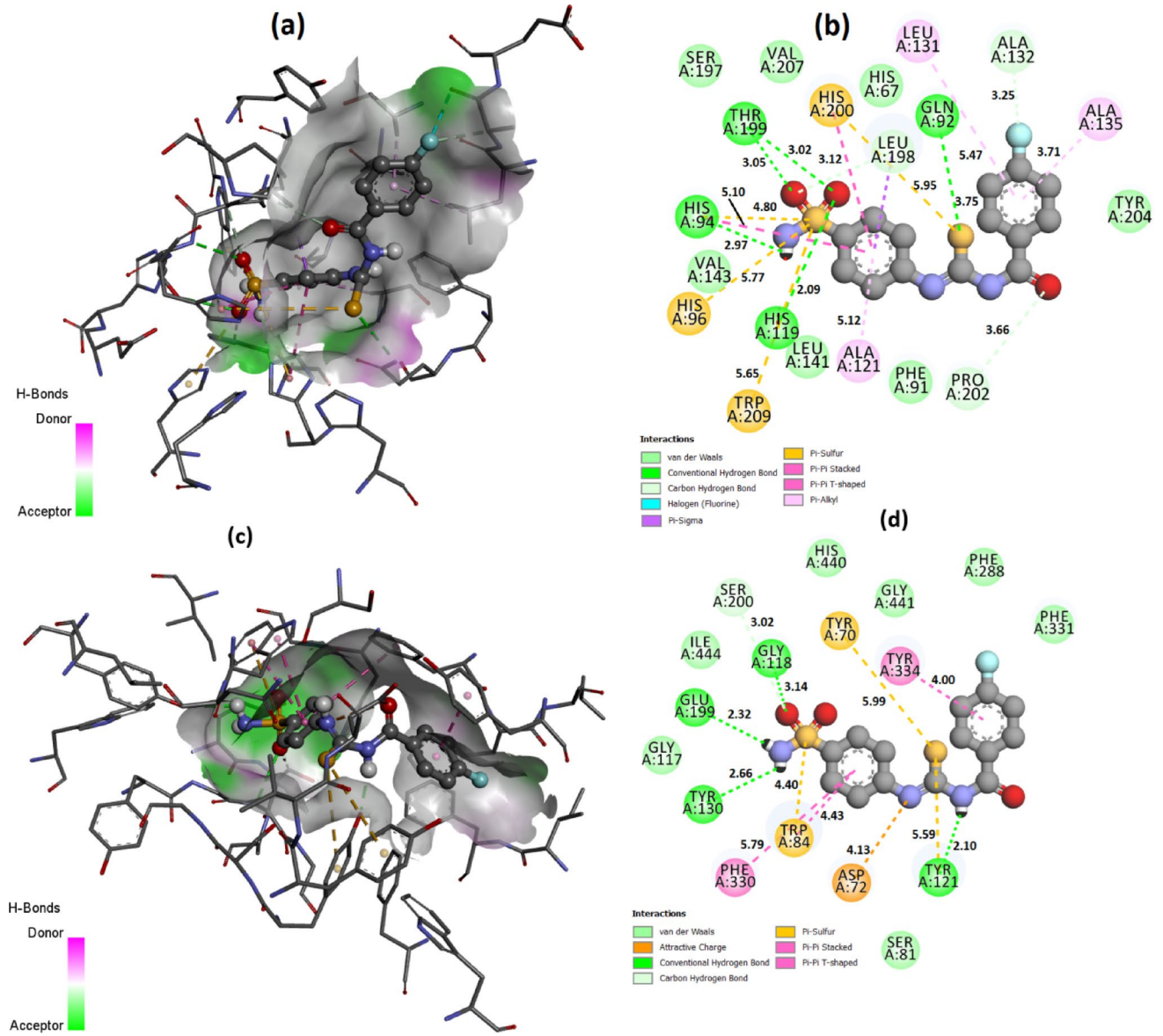


Fig. 4 The 3D (**a**, **c**) and 2D (**b**, **d**) molecular docking results for compound **M1** and PDBs: 2CAB and 1EVE

favorable interactions in the docking poses. While the present study did not aim to construct a quantitative correlation model, the observed consistency between binding energies and biological activities supports the predictive value of the docking analyses and reinforces the experimental findings.

Optimization and MEP analysis-DFT

One popular quantum mechanical method for examining the electrical structure of molecules and materials is density functional theory, or DFT. Because it strikes a compromise between accuracy and computational efficiency, it is perfect for modeling chemical characteristics. The Lee-Yang-Parr correlation functional (LYP) and Becke's three-parameter exchange functional (B3) are combined to create the B3LYP functional, a hybrid exchange-correlation functional. Because of its consistent ability to predict molecule geometries, energy, and reaction routes, B3LYP is widely used. Polarization functions (d, p) and diffuse functions (++) are included in the 6-311++G(d, p) basis set, a split-valence triple-zeta basis set that improves the description of electron distribution, especially for anions and systems containing lone pairs. When combined, DFT with the 6-311++G(d, p) basis set and the B3LYP functional provides a strong framework for precisely optimizing molecular structures and analyzing electronic properties (Becke 1993; Krishnan et al. 1980). Additionally, Molecular Electrostatic Potential (MEP) maps provide critical insights into the electrophilic

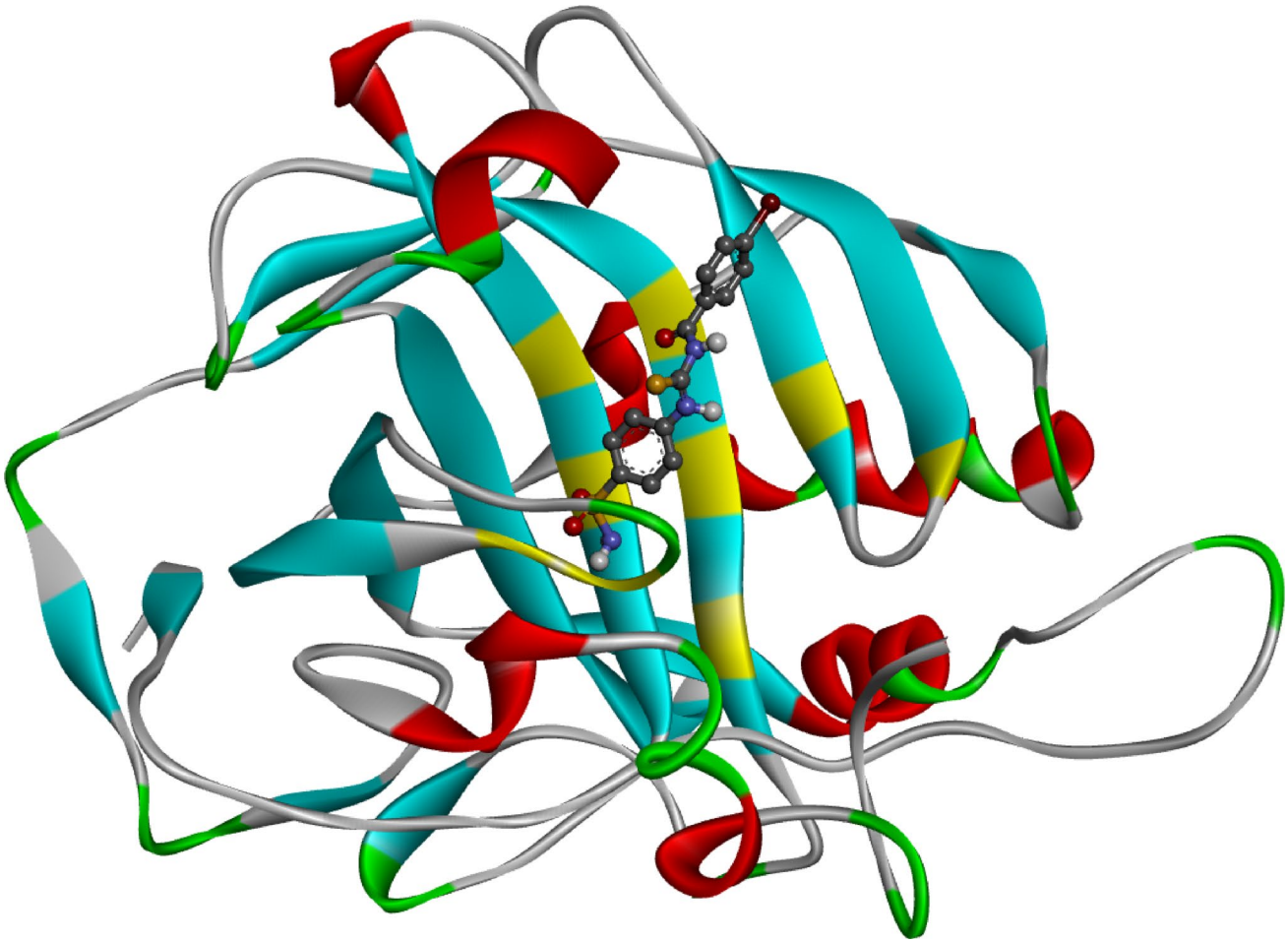


Fig. 5 The localization of the molecule **M9** to the active site of the protein 5AML

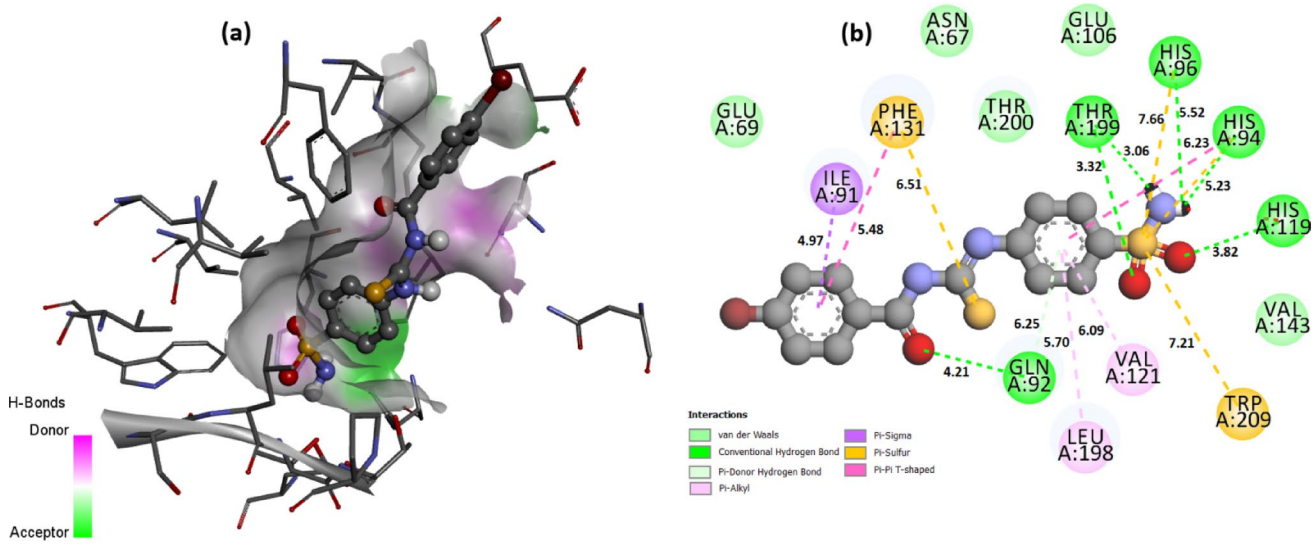


Fig. 6 The 3D (**a**) and 2D (**b**) molecular docking results for compound **M9** and PDB: 5AML

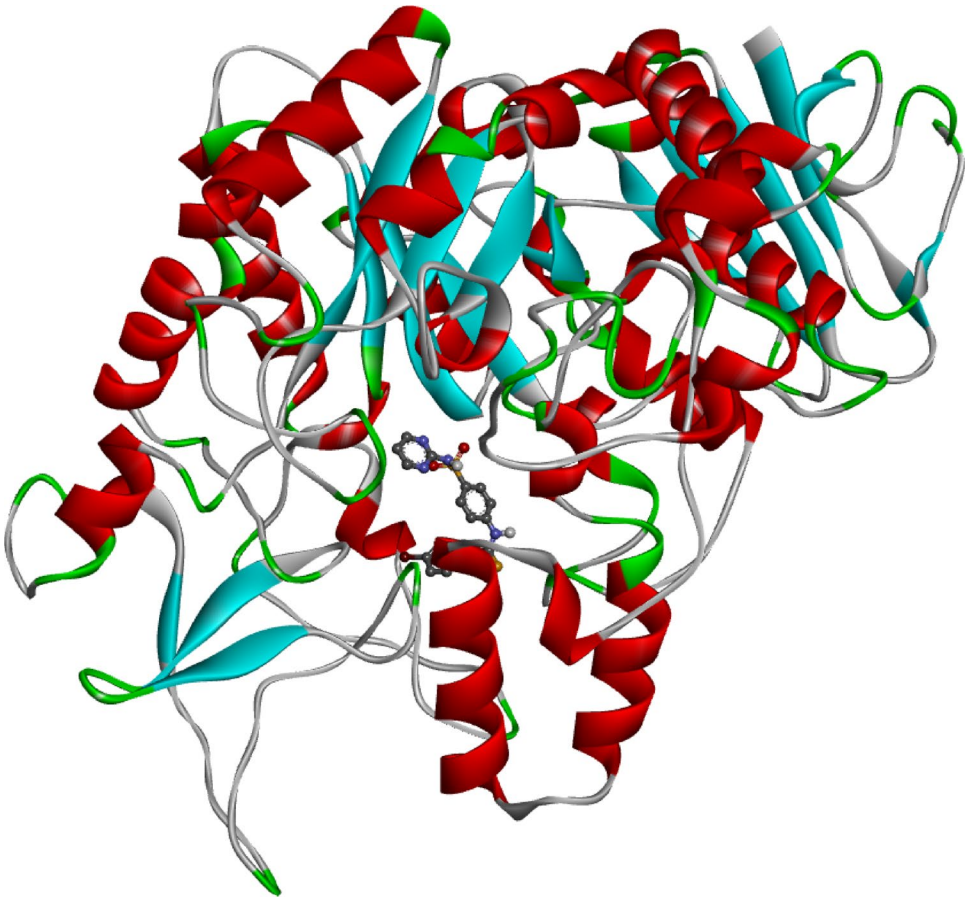


Fig. 7 The localization of the molecule **M10** to the active site of the protein 3A4A

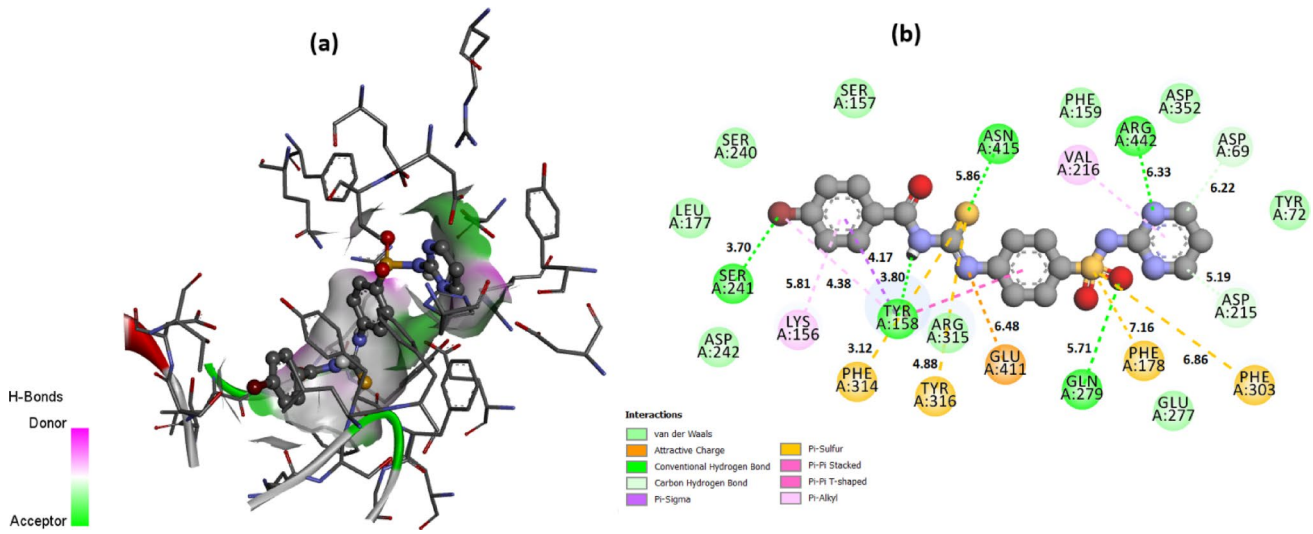


Fig. 8 The 3D (**a**) and 2D (**b**) molecular docking results for compound **M10** and PDB: 3A4A

and nucleophilic regions of molecules, which are essential for understanding how ligands interact with target proteins. By identifying reactive sites, MEP analysis complements molecular docking studies, helping to predict binding affinities and optimize inhibitor design (Politzer and Truhlar 2013; Murray and Politzer 2011).

In this section, firstly, the molecules **M1**, **M9**, **M10** and **M17** were quantum chemically optimized in the gas phase using Gaussian 09 W and GaussView 5.0 programs with the above-mentioned theory, functional, and basis set, and their 3D ideal forms were obtained as shown in Fig. 11. As a result of the calculation, the sum of electronic and zero point

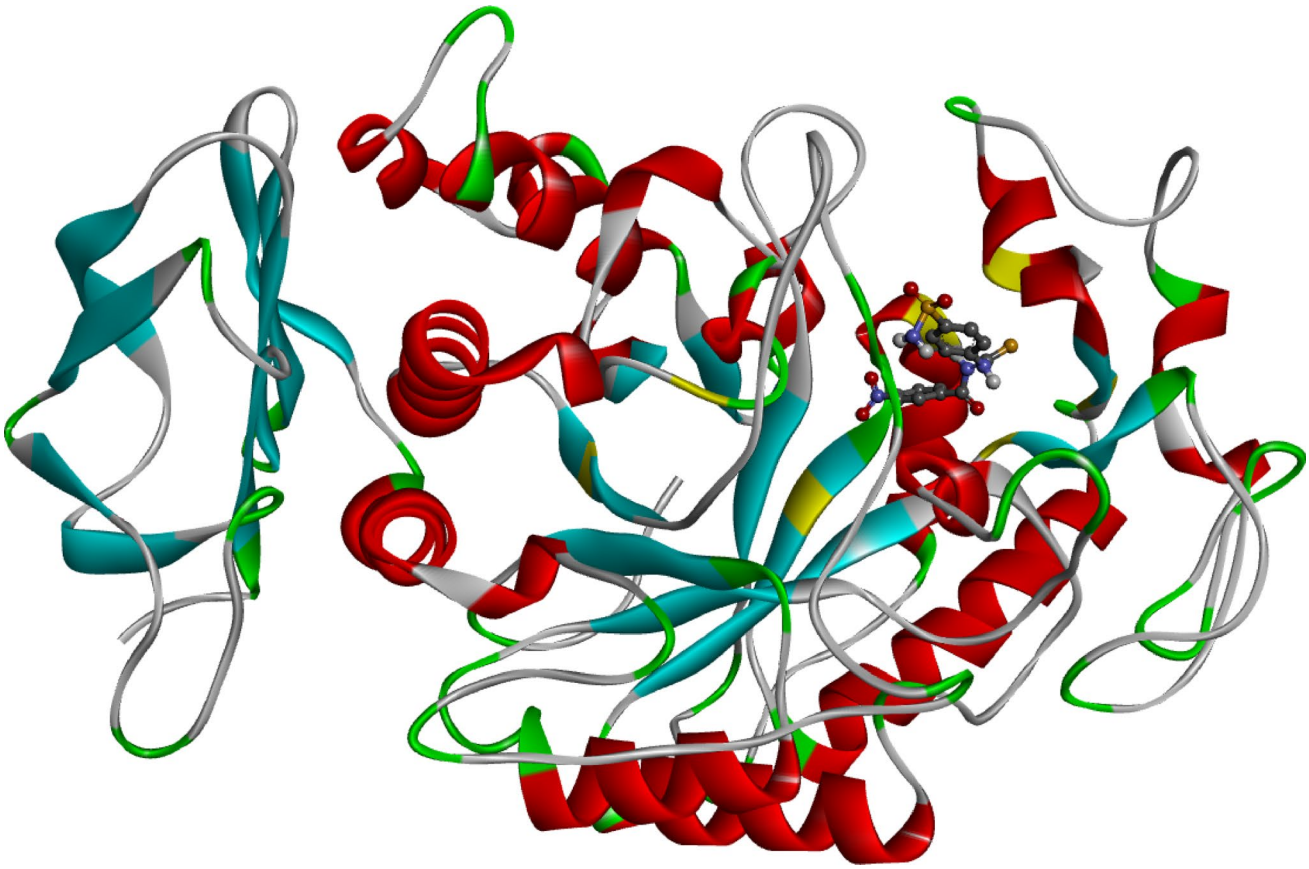


Fig. 9 The localization of the molecule **M17** to the active site of the protein 1SMD

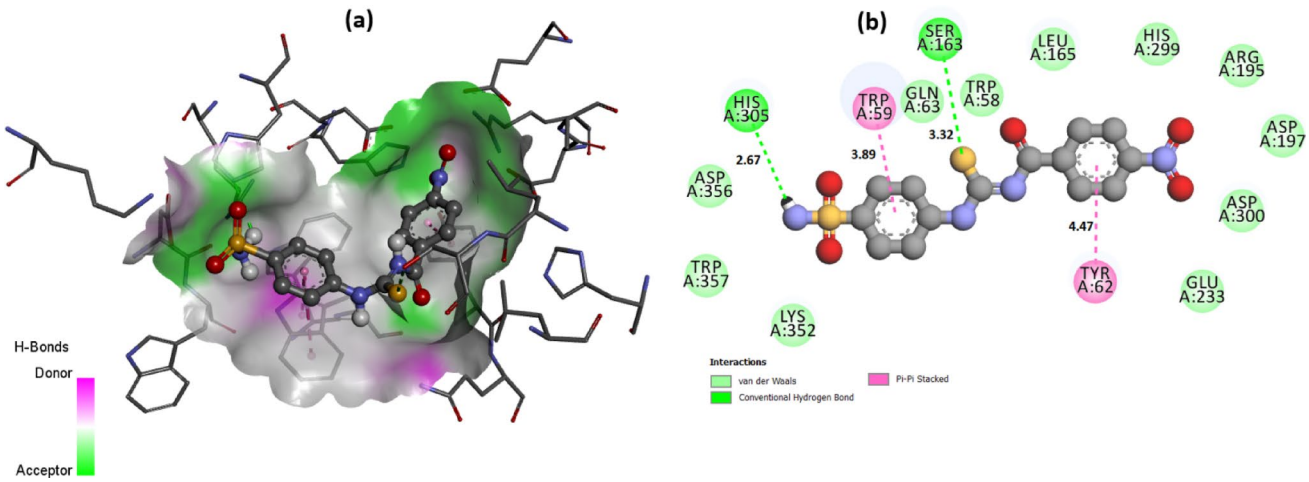


Fig. 10 The 3D (**a**) and 2D (**b**) molecular docking results for compound **M17** and PDB: 1SMD

energies were found as -1817.10739324, -4279.61421494, -4541.29651619 and −1921.74613079 a.u., respectively. Subsequently, the MEP (molecular Electrostatic Potential Surfaces and MEP scales) were obtained by optimizing the molecules and using the generated chk* files as shown in Fig. 12. This figure presents the molecular electrostatic potential (MEP) surfaces and corresponding MEP scales for four distinct molecules: (a) **M1**, (b) **M9**, (c) **M10**, and (d) **M17**. The MEP maps visualize regions of electrostatic potential using a color gradient, providing insights into the electrophilic and nucleophilic reactivity of each molecule. The MEP surfaces are color-coded on a scale ranging from red to blue. Red regions represent areas of negative electrostatic potential, indicating electron-rich zones prone to

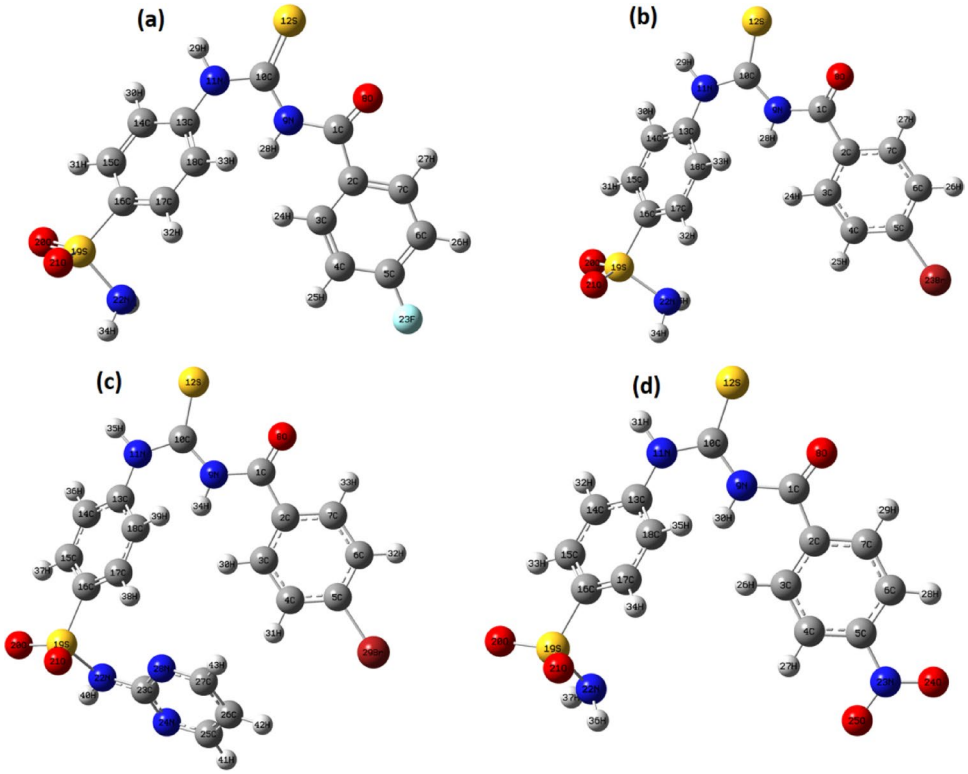


Fig. 11 The optimized structures of **M1**, **M9**, **M10** and **M17** molecules

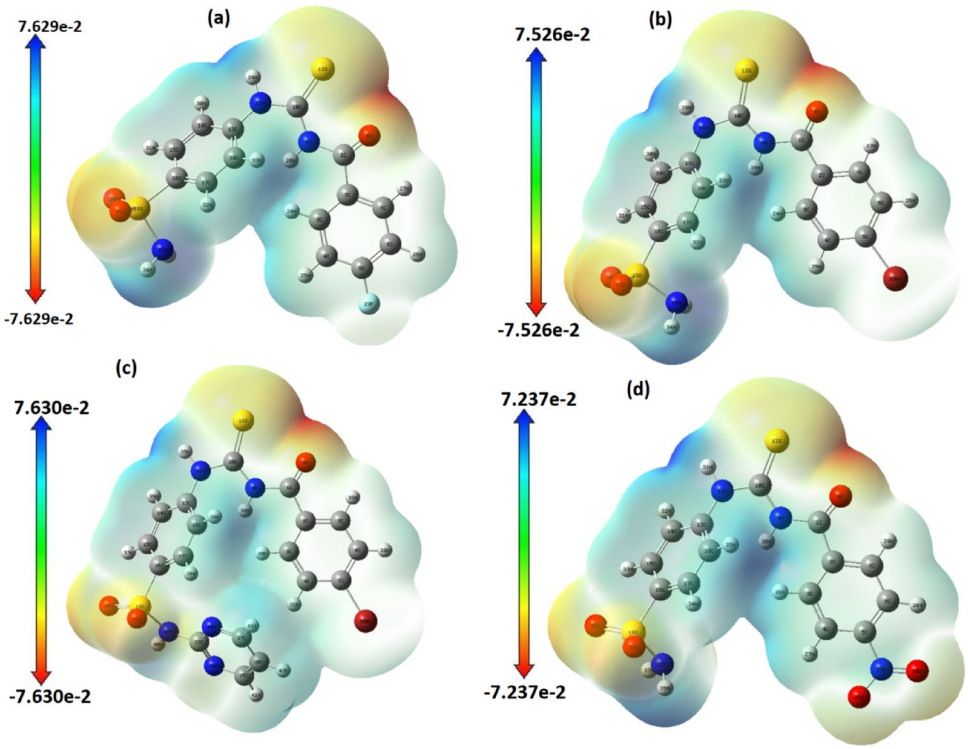


Fig. 12 The MEP surfaces of **M1**, **M9**, **M10** and **M17** molecules

electrophilic attack. In contrast, blue regions represent areas of positive electrostatic potential, highlighting electron-deficient zones susceptible to nucleophilic attack. Each molecule exhibits distinct electrostatic potential distributions. Molecule **M1** (a) displays both nucleophilic (blue) and electrophilic (red) regions, with significant negative potential near oxygen and nitrogen atoms due to their high electronegativity. Molecule **M9** (b) shows a similar pattern, but the extent of negative potential is slightly reduced compared to **M1**, suggesting differences in electron distribution.

Molecule **M10** (c) has a pronounced concentration of negative potential around its functional groups, indicating higher susceptibility to electrophilic interactions. In contrast, Molecule **M17** (d) shows a more balanced potential distribution, with a slightly lower magnitude of electrostatic potential compared to the other molecules. The MEP scales for each molecule range approximately from $\pm 7.2e^{-2}$ to $\pm 7.6e^{-2}$. Molecules **M1** and **M10** have the widest potential ranges ($\pm 7.629e^{-2}$ and $\pm 7.630e^{-2}$, respectively), indicating stronger reactivity potential compared to **M9** ($\pm 7.526e^{-2}$) and M17 ($\pm 7.237e^{-2}$). The distribution of electrophilic (red) and nucleophilic (blue) points is influenced by specific functional groups, particularly the presence of oxygen, nitrogen, and sulfur atoms. These atoms contribute to the electron density due to their ability to donate or withdraw electrons. In conclusion, these MEP surfaces effectively illustrate the electronic characteristics of each molecule, highlighting regions susceptible to electrophilic and nucleophilic interactions. Comparing these molecules provides valuable insights into their electronic distribution and potential reactivity, aiding in the prediction of their behavior in chemical reactions.

The MEP analyses reveal that the lead compounds showing the highest inhibitory activity experimentally also present the most negative electrostatic potential regions on their molecular surfaces. For example, **M1** and **M9** display deeper electron-rich regions around the thiocarbonyl and sulfonamide groups, consistent with their strong interactions in hCA I, hCA II and AChE active sites. These negative potential zones correspond to the regions involved in hydrogen bonding and electrostatic contacts in the docking studies, providing a rational explanation for their higher binding affinities. In contrast, the less active compound **M17** exhibits weaker MEPminima, consistent with its lower stabilizing interactions. These observations indicate that the electrostatic characteristics identified by MEP mapping contribute to the observed variations in biological activity among the lead molecules.

The observed nanomolar inhibitory activity against both enzymes can be attributed to the incorporation of distinct pharmacophoric elements within the molecular framework. These elements are capable of independently engaging different catalytic environments, thereby supporting a multitarget-directed ligand strategy rather than implying structural similarity between the enzymes.

Drug-likeness properties

As a last step, in order to predict whether the leading compounds have drug-likeness properties, it was investigated whether these compounds obey Lipinski rules (Lipinski 2000). The theoretical results were calculated with SwissADME The results are within the theoretical limits, it can be stated that the compounds are drug-like (Daina et al. 2017). The in silico ADME analysis revealed that all compounds complied with Lipinski's rule of five, suggesting acceptable drug-likeness in terms of molecular weight, hydrogen bond donors/acceptors and lipophilicity. However, all molecules exhibited low predicted gastrointestinal absorption and lacked blood-brain barrier permeability. **M10** and **M17** showed less favorable pharmacokinetic profiles due to their higher molecular weight, elevated topological polar surface area and failure to meet multiple drug-likeness filters, indicating potential limitations in oral bioavailability (Table 5).

Conclusions

In this present study, a series of thiourea and thiazolidinone derivatives (**M1-M20** and **MD1-MD4**) were synthesized and screened for their enzyme inhibitory effects. The enzyme inhibition and molecular docking studies obtained show that the lead compounds are more effective than the reference drugs. While the most potent inhibitory compound in the series against hCA I enzyme was **M1** ($Ki = 19.88 \pm 1.04$ nM), the most potent compound against hCA II enzyme was **M9** ($Ki = 8.9890 \pm 0.8909$ nM). It was shown that most of the compounds showed moderate to good inhibitory potentials on screening against AChE with Ki values ranging from 0.4740 ± 0.0818 nM to 22.7715 ± 7.1975 nM. Compound **M1** was the strongest inhibitor in the series with a Ki value of 0.4740 ± 0.0818 nM against AChE. Compound **M10** also showed good potency against the α-glucosidase enzyme. In the case of α-amylase inhibition, compound **M17** showed promising inhibitory potency with an IC_{50} value of 12.044 nM. The most potent compounds were subjected to molecular docking analyses in order to elucidate the potential mechanisms of interaction with the active sites of their respective enzymes. The integration of docking, DFT calculations, and MEP analysis provided a robust framework for the design of effective and selective therapeutic agents in the future.

Experimental

Chemistry

Nuclear magnetic resonance (NMR) spectra (^{1}H NMR and ^{13}C NMR) of the compounds were taken using Varian (400 MHz, Danbury, USA) spectrometer. High Resolution Mass Spectra (HRMS) equipped with an electrospray ionization (ESI) source and a liquid chromatography ion trap-time of the flight tandem mass spectrometer (Shimadzu,

Table 5 Druglikeness properties of the potent compounds

Descriptors	Compound M1	Compound M9	Compound M10	Compound M17
Formula	$C_{14}H_{12}N_3O_3FS_2$	$C_{14}H_{12}N_3O_3S_2Br$	$C_{18}H_{14}N_5O_3S_2Br$	$C_{14}H_{12}N_4O_5S_2$
MW (g/mol)	353.39	414.30	492.37	380.40
Rotatable bonds	6	6	8	7
HBA	5	4	5	6
HBD	3	3	3	3
MR	87.01	94.75	116.46	95.87
TPSA Å²	141.76	141.76	153.55	187.58
Mean Log P	2.06	2.31	2.75	0.93
GI absorption	Low	Low	Low	Low
BBB permanent	No	No	No	No
Lipinski RO5	Yes	Yes	Yes	Yes
Ghose	Yes	Yes	No[1]	Yes
Veber	No[1]	No[1]	No[1]	No[1]
Egan	No[1]	No[1]	No[1]	No[1]
Muegge	Yes	Yes	No[1]	No[1]

Lipinski filter: MW ≤ 500; MLOGP ≤ 4.15; HBA ≤ 10; HBD ≤ 5

Ghose filter: 160 ≤ MW ≤ 480; − 0.4 ≤ WLOGP ≤ 5.6; 40 ≤ MR ≤ 130; 20 ≤ atoms ≤ 70

Veber filter: Rotatable bonds ≤ 10; TPSA ≤ 140 Å2

Egan filter: WLOGP ≤ 5.88; TPSA ≤ 131.6

Muegge filter: 200 ≤ MW ≤ 600, − 2 ≤ XLOGP ≤ 5; TPSA ≤ 157; HBA ≤ 10; HBD ≤ 5; RB ≤ 15; Number of rings ≤ 7; Number of carbons > 4; Number of heteroatoms > 1

No;[1] violation: TPSA > 140, TPSA > 131.6, MW > 480, TPSA > 150

Kyoto, Japan) was used for HRMS analysis. Melting points of the compounds were determined by Electrothermal 9100 instrument (IA9100, Bibby Scientific Limited, Staffordshire, UK) device. Thin Layer Chromatography (TLC) by Silicagel HF254 (Merck Art 5715) plate under UV lamb (254 and 365 nm, Spectroline, Model ENF-240 C/ FE, Spectronics Corporation Westbury, New York U.S.A) was used to monitor the reaction progress. DMSO-d_6 was used as NMR solvent.

General procedure for the synthesis of compounds M1-M20 (Scheme 1)

A solution of substituted benzoyl chloride (1 mmol) in acetone (20 ml) was added dropwise to a suspension of potassium thiocyanate (1 mmol) in acetone (30 ml), and the reaction mixture was refluxed for 1.5 h. The reaction mixture was checked with TLC and benzoyl isothiocyanate derivative was formed in a reaction medium. After completion of the reaction, the substituted sulfonamide derivative (1 mmol) was added and the mixture was stirred under reflux for 4 – 8 h. Upon completion of the reaction (checked with TLC), the resulting precipitate was collected by filtration and recrystallized from dimethylformamide/ethanol/H_2O (4.2:0.6:0.2) to obtain the pure products **M1-M20** (Mahdavi et al. 2014; Tugrak et al. 2021c).

4-Fluoro-*N*-[(4-sulfamoylphenyl)carbamothioyl]benzamide (M1)

White color solid, mp: 215 – 216 °C, yield 80%. ^{1}H NMR (DMSO-d_6, ppm, 400 MHz), δ 12.67 (s, 1H, NH), 11.76 (s, 1H, NH), 8.09 – 8.06 (m, 2H, Ar-H), 7.92 – 7.85 (m, 3H, Ar-H), 7.42 – 7.37 (m, 5H, Ar-H, NH_2); ^{13}C NMR (DMSO-d_6, ppm, 100 MHz) δ 179.9 (C = S), 167.6 (C = O),166.7, 164.2, 141.8, 132.3, 129.1, 126.8, 124.8, 116.1; HRMS (ESI-MS) $C_{14}H_{12}N_3O_3FS_2$; calculated $[M+H]^+$: 354.0377; found $[M+H]^+$: 354.0388.

4-Fluoro-*N*-({4-[*N*-(pyrimidin-2-yl)sulfamoyl]phenyl} carbamothioyl)benzamide (M2)

White color solid, mp: 240 – 241 °C, yield 86%. ^{1}H NMR (DMSO-d_6, ppm, 400 MHz), δ 12.69 (s, 1H, NH), 11.75 (s, 1H, NH), 8.54 – 8.48 (m, 2H, Ar-H), 8.08 – 7.95 (m, 7H, Ar-H, NH), 7.40 – 7.36 (m, 2H, Ar-H), 7.08 – 7.06 (m, 1H, Ar-H); ^{13}C NMR (DMSO-d_6, ppm, 100 MHz) δ 179.2 (C = S), 166.9 (C = O), 166.2, 163.7, 158.3, 156.8, 141.8, 137.3, 131.8, 128.2, 123.8, 115.6, and 115.4; HRMS (ESI-MS) $C_{18}H_{14}N_5O_3FS_2$; calculated $[M+H]^+$: 432.0595; found $[M+H]^+$: 432.0612.

4-Fluoro-*N*-({4-[*N*-(4-methylpyrimidin-2-yl)sulfamoyl] phenyl}carbamothioyl)benzamide (M3)

Light cream color solid, mp: 235 – 236 °C, yield 86%. ^{1}H NMR (DMSO-d_6, ppm, 400 MHz), δ 12.69 (s, 1H, NH), 11.75 (s, 1H, NH), 8.32 (dd, 1H, Ar-H, J=9.8, 4.5 Hz), 8.08 – 7.93 (m, 7H, Ar-H, NH), 7.40 – 7.36 (m, 2H, Ar-H), 6.92 – 6.91 (m, 1H, Ar-H), 2.33 (s, 3H, CH_3); ^{13}C NMR (DMSO-d_6, ppm, 100 MHz) δ 179.2 (C=S), 166.9 (C=O), 166.2, 163.7, 156.4, 141.6, 137.5, 131.8, 131.7, 128.4, 123.6, 115.6, 115.4, 23.2; HRMS (ESI-MS) $C_{19}H_{16}N_5O_3FS_2$; calculated $[M+H]^+$: 446.0751; found $[M+H]^+$: 446.0771.

4-Fluoro-*N*-({4-[*N*-(4,6-dimethylpyrimidin-2-yl)sulfamoyl] phenyl}carbamothioyl)benzamide (M4)

White color solid, mp: 210 – 211 °C, yield 84%. ^{1}H NMR (DMSO-d_6, ppm, 400 MHz), δ 12.69 (s, 1H, NH), 11.74 (s, 1H, NH), 8.08 – 8.01 (m, 5H, Ar-H), 7.92 (d, 2H, Ar-H, J=7.2 Hz), 7.40 – 7.35 (m, 2H, Ar-H), 6.76 (s, 1H, NH), 2.26 (s, 6H, 2xCH_3); ^{13}C NMR (DMSO-d_6, ppm, 100 MHz) δ 179.1 (C=S), 167.0 (C=O), 166.2, 163.7, 155.9, 141.4, 137.9, 131.8, 131.7, 128.7, 123.4, 115.6, 115.4, and 22.7; HRMS(ESI-MS) $C_{20}H_{18}N_5O_3FS_2$; calculated $[M+H]^+$: 460.0908; found $[M+H]^+$: 460.0924.

4-Chloro-*N*-[(4-sulfamoylphenyl)carbamothioyl]benzamide (M5)

Light white color solid, mp: 225 – 226 °C, yield 85%. ^{1}H NMR (DMSO-d_6, ppm, 400 MHz), δ 12.66 (s, 1H, NH), 11.79 (s, 1H, NH), 8.00 (d, 2H, Ar-H, J=8.6 Hz), 7.93 – 7.86 (m, 4H, Ar-H), 7.60 (d, 2H, Ar-H, J=8.6 Hz), 7.42 (bs, 2H, NH_2); ^{13}C NMR (DMSO-d_6, ppm, 100 MHz) δ 179.8 (C=S), 167.7 (C=O),141.8, 141.3, 138.6, 131.3, 131.2, 129.0, 126.8, 124.8; HRMS (ESI-MS) $C_{14}H_{12}N_3O_3S_2Cl$; calculated $[M+H]^+$: 370.0081; found $[M+H]^+$: 370.0096.

4-Chloro-*N*-({4-[*N*-(pyrimidin-2-yl)sulfamoyl]phenyl} carbamothioyl)benzamide (M6)

Cream color solid, mp: 245 – 246 °C, yield 77%. ^{1}H NMR (DMSO-d_6, ppm, 400 MHz), δ 12.66 (s,1H, NH), 11.78 (s, 1H, NH), 8.51 (d, 2H, Ar-H, J=4.8 Hz), 8.04 – 7.95 (m, 7H, Ar-H, NH), 7.60 (d, 2H, Ar-H, J=8.5 Hz), 7.06 – 7.04 (m, 1H, Ar-H); ^{13}C NMR (DMSO-d_6, ppm, 100 MHz) δ 179.6 (C=S), 167.6 (C=O), 158.8, 157.3, 142.3, 138.6, 137.8, 131.3, 131.2, 128.9, 128.8, 124.3 116.3; HRMS (ESI-MS) $C_{18}H_{14}N_5O_3S_2Cl$; calculated $[M+H]^+$: 448.0299; found $[M+H]^+$: 448.0305.

4-Chloro-*N*-({4-[*N*-(4-methylpyrimidin-2-yl)sulfamoyl] phenyl}carbamothioyl)benzamide (M7)

Dark cream color solid, mp: 242 – 244 °C, yield 70%. ^{1}H NMR (DMSO-d_6, ppm, 400 MHz), δ 12.67 (s, 1H, NH), 11.79 (s, 1H, NH), 8.33 (d, 1H, Ar-H, J=5.1 Hz), 8.05 – 7.94 (m, 7H, Ar-H, NH), 7.58 (d, 2H, Ar-H, J=8.4 Hz), 6.88 (d, 1H, Ar-H, J=5.1 Hz), 2.31 (s, 3H, CH_3); ^{13}C NMR (DMSO-d_6, ppm, 100 MHz) δ 179.6 (C=S), 168.8 (C=O), 167.6, 157.9, 156.9, 142.1, 138.6, 138.0, 131.3, 131.1, 129.2, 128.9, 124.1, 115.2, 23.7; HRMS (ESI-MS) $C_{19}H_{16}N_5O_3S_2Cl$; calculated $[M+H]^+$: 462.0456; found $[M+H]^+$: 462.0476.

4-Chloro-*N*-({4-[*N*-(4,6-dimethylpyrimidin-2-yl)sulfamoyl] phenyl}carbamothioyl)benzamide (M8)

Cream color solid, mp: 215 – 217 °C, yield 71%. ^{1}H NMR (DMSO-d_6, ppm, 400 MHz), δ 12.66 (s, 1H, NH), 11.78 (s, 1H, NH), 8.04 – 7.91 (m, 7H, Ar-H, NH), 7.59 (d, 2H, Ar-H, J=8.5 Hz), 6.73 (s, 1H, NH), 2.32 (s, 6H, 2xCH_3); ^{13}C NMR (DMSO-d_6, ppm, 100 MHz) δ 179.6 (C=S), 167.6 (C=O), 156.5, 141.8, 138.6, 138.2, 131.3, 131.2, 131.0, 129.2, 128.9, 123.9, 113.7, 23.2; HRMS (ESI-MS) $C_{20}H_{18}N_5O_3S_2Cl$; calculated $[M+H]^+$: 476.0612; found $[M+H]^+$: 476.0635.

4-Bromo-*N*-[(4-sulfamoylphenyl)carbamothioyl]benzamide (M9)

White color solid, mp: 234 – 235 °C, yield 83%. ^{1}H NMR (DMSO-d_6, ppm, 400 MHz), δ 12.62 (s, 1H, NH), 11.79 (s, 1H, NH), 7.93 – 7.85 (m, 6H, Ar-H), 7.77 – 7.75 (d, 2H, Ar-H, J=8,5 Hz), 7.41 (s, 2H, NH); ^{13}C NMR (DMSO-d_6, ppm, 100 MHz) δ 179.8 (C=S), 167.8 (C=O), 141.8, 141.3, 131.9, 131.8, 131.3, 127.7, 126.8, 124.9; HRMS (ESI-MS) $C_{14}H_{12}N_3O_3S_2Br$; calculated $[M+H]^+$: 413.9576; found $[M+H]^+$: 413.9579.

4-Bromo-*N*-({4-[*N*-(pyrimidin-2-yl)sulfamoyl]phenyl} carbamothioyl)benzamide (M10)

Cream color solid, mp: 245 – 247 °C, yield 78%. ^{1}H NMR (DMSO-d_6, ppm, 400 MHz), δ 12.65 (s, 1H, NH), 11.78 (s, 1H, NH), 8.54 – 8.48 (m, 2H, Ar-H), 8.08 – 7.95 (m, 7H, Ar-H, NH), 7.40 – 7.36 (m, 2H, Ar-H), 7.08 – 7.06 (m, 1H, Ar-H); ^{13}C NMR (DMSO-d_6, ppm, 100 MHz) δ 179.6 (C=S), 167.7 (C=O), 158.8, 157.3, 142.3, 137.8, 131.9, 131.7, 131.3, 128.8, 127.7, 124.3, 116.3; HRMS (ESI-MS) $C_{18}H_{14}N_5O_3S_2Br$; calculated $[M+H]^+$: 491.9794; found $[M+H]^+$: 491.9808.

4-Bromo-*N*-({4-[*N*-(4-methylpyrimidin-2-yl)sulfamoyl] phenyl}carbamothioyl)benzamide (M11)

Dark cream color solid, mp: 246 – 247 °C, yield 75%. ^{1}H NMR (DMSO-d_6, ppm, 400 MHz), δ 12.63 (s, 1H, NH), 11.78 (s, 1H, NH), 8.32 (d, 1H, Ar-H, J=5.1 Hz), 8.03 – 7.89 (m, 7H, Ar-H, NH), 7.75 (d, 2H, Ar-H, J=8.5 Hz), 6.90 (d, 1H, Ar-H, J=5.1 Hz), 2.32 (s, 3H, CH_3); ^{13}C NMR (DMSO-d_6, ppm, 100 MHz) δ 179.6 (C=S), 167.7 (C=O), 156.9, 153.2, 142.1, 138.1, 131.9, 131.7, 131.3, 130.5, 128.9, 127.7, 124.1, 115.2, 23.7; HRMS (ESI-MS) $C_{19}H_{16}N_5O_3S_2Br$; calculated $[M+H]^+$: 505.9951; found $[M+H]^+$: 505.9962.

4-Bromo-*N*-({4-[*N*-(4,6-dimethylpyrimidin-2-yl)sulfamoyl] phenyl}carbamothioyl)benzamide (M12)

Light yellow color solid, mp: 217 – 219 °C, yield 70%. ^{1}H NMR (DMSO-d_6, ppm, 400 MHz), δ 12.68 (s, 1H, NH), 11.77 (s, 1H, NH), 8.06 – 8.03 (m, 2H, Ar-H), 7.94 – 7.88 (m, 5H, Ar-H), 7.72 (d, 2H, Ar-H, J=8.3 Hz), 6.70 (s, 1H, NH), 2.32 (s, 6H, 2xCH_3); ^{13}C NMR (DMSO-d_6, ppm, 100 MHz) δ 179.5 (C=S), 167.8 (C=O), 156.5, 141.8, 138.5, 131.9, 131.7, 131.6, 131.2, 129.2, 127.7, 123.9, 113.6, 23.2; HRMS (ESI-MS) $C_{20}H_{18}N_5O_3S_2Br$; calculated $[M+H]^+$: 520.0107; found $[M+H]^+$: 520.0122.

4-Methoxy-*N*-[(4-sulfamoylphenyl)carbamothioyl] benzamide (M13)

White color solid, mp: 217 – 219 °C, yield 82%. ^{1}H NMR (DMSO-d_6, ppm, 400 MHz), δ 12.87 (s, 1H, NH), 11.50 (s, 1H, NH), 8.03 (d, 2 H, Ar-H, J=8.8 Hz), 7.93 – 7.85 (m, 3H, Ar-H), 7.41 (s, 2H, Ar-H, NH), 7.07 (d, 2H, Ar-H, J=8.9 Hz), 3.85 (s, 3H, CH_3O); ^{13}C NMR (DMSO-d_6, ppm, 100 MHz) δ 179.9 (C=S), 167.9 (C=O), 163.8, 141.7, 141.4, 131.5, 126.7, 124.8, 124.2, 114.3, 56.1; HRMS (ESI-MS) $C_{15}H_{15}N_3O_4S_2$; calculated $[M+H]^+$: 366.0577; found $[M+H]^+$: 366.0579.

4-Methoxy-*N*-({4-[*N*-(pyrimidin-2-yl)sulfamoyl]phenyl} carbamothioyl)benzamide (M14)

Yellow color solid, mp: 245 – 246 °C, yield 76%. ^{1}H NMR (DMSO-d_6, ppm, 400 MHz), δ 12.90 (s, 1H, NH), 11.52 (s, 1H, NH), 8.51 (d, 2H, Ar-H, J=4.8 Hz), 8.47 – 7.96 (m, 6H, Ar-H), 7.06 – 6.99 (m, 4H, Ar-H, NH), 3.83 (s, 3H, OCH_3); ^{13}C NMR (DMSO-d_6, ppm, 100 MHz) δ 179.8 (C=S), 167.9 (C=O), 163.8, 158.8, 157.3, 142.4, 137.6, 131.8, 130.8, 128.7, 124.2, 116.3, 114.3, 56.1; HRMS (ESI-MS) $C_{19}H_{17}N_5O_4S_2$; calculated $[M+H]^+$: 444.0795; found $[M+H]^+$: 444.0800.

4-Methoxy-*N*-({4-[*N*-(4-methylpyrimidin-2-yl)sulfamoyl] phenyl}carbamothioyl)benzamide (M15)

Dark yellow color solid, mp: 232 – 233 °C, yield 74%. ^{1}H NMR (DMSO-d_6, ppm, 400 MHz), δ 12.93 (s, 1H, NH), 11.51 (s, 1H, NH), 8.38 (d, 1H, Ar-H, J=5.1 Hz), 8.33 – 7.15 (m, 7H, Ar-H, NH), 7.04 (d, 2H, Ar-H, J=8.8 Hz), 6.88 (d, 1H, Ar-H, J=5.1 Hz), 3.82 (s, 3H, OCH_3), 2.31 (s, 3H, CH_3); ^{13}C NMR(DMSO-d_6, ppm, 100 MHz) δ 179.8 (C=S), 167.9 (C=O), 167.5, 163.8, 162.7, 156.9, 142.2, 137.9, 131.8, 131.5, 128.9, 124.0, 115.2, 114.2, 56.0, 23.6; HRMS (ESI-MS) $C_{20}H_{19}N_5O_4S_2$; calculated $[M+H]^+$: 458.0951; found $[M+H]^+$: 458.0965.

4-Methoxy-*N*-({4-[*N*-(4,6-dimethylpyrimidin-2-yl)sulfamoyl] phenyl}carbamothioyl)benzamide (M16)

Yellow color solid, mp: 214 – 216 °C, yield 68%. ^{1}H NMR (DMSO-d_6, ppm, 400 MHz), δ 12.91 (s, 1H, NH), 11.49 (s, 1H, NH), 8.04 – 7.93 (m, 7H, Ar-H), 7.03 (d, 2H, Ar-H, J=8.8 Hz), 6.72 (s, 1H, NH), 3.83 (s, 3H, OCH_3), 2.32 (s, 6H, 2xCH_3); ^{13}C NMR (DMSO-d_6, ppm, 100 MHz) δ 179.8 (C=S), 167.9 (C=O), 163.8, 156.5, 141.9, 138.3, 131.5, 130.1, 129.2, 124.1, 123.8, 114.3, 113.7, 56.0, 23.2; HRMS (ESI-MS) $C_{21}H_{21}N_5O_4S_2$; calculated $[M+H]^+$: 472.1108; found $[M+H]^+$: 472.1121.

4-Nitro-*N*-[(4-sulfamoylphenyl)carbamothioyl]benzamide (M17)

Yellow color solid, mp: 192 – 193 °C, yield 80%. ^{1}H NMR (DMSO-d_6, ppm, 400 MHz), δ 12.50 (s, 1H, NH), 11.93 (s, 1H, NH), 8.35 (d, 2H, Ar-H, J=8.7 Hz), 8.18 – 8.15 (m, 4H, Ar-H), 8.13 – 7.86 (m, 2H, Ar-H) 7.41 (s, 2H, NH) ; ^{13}C NMR (DMSO-d_6, ppm, 100 MHz) δ 179.6 (C=S), 167.04 (C=O), 150.3, 141.9, 141.3, 139.7, 138.5, 130.8, 126.8, 123.8; HRMS(ESI-MS) $C_{14}H_{12}N_4O_5S_2$; calculated $[M+H]^+$: 381.0322; found $[M+H]^+$: 381.0322.

4-Nitro-*N*-({4-[*N*-(pyrimidin-2-yl)sulfamoyl]phenyl} carbamothioyl)benzamide (M18)

Dark yellow color solid, mp: 237 – 239 °C, yield 67%. ^{1}H NMR (DMSO-d_6, ppm, 400 MHz), δ 12.52 (s, 1H, NH), 12.01 (s, 1H, NH), 8.52 (d, 2H, Ar-H, J=4.8 Hz), 8.34 (d, 2H, Ar-H, J=8.8 Hz), 8.16 (d, 2H, Ar-H, J=8.8 Hz), 8.03 (d, 2H, Ar-H, J=8.7 Hz), 7.95 (d, 2H, Ar-H, J=8.7 Hz), 7.06 (t, 2H, Ar-H, J=4.8 Hz), ^{13}C NMR (DMSO-d_6, ppm, 100 MHz) δ 179.4 (C=S), 166.9 (C=O), 158.8, 157.3, 150.3, 142.3, 138.4, 137.8, 130.8, 128.8, 124.3, 123.8, 116.3; HRMS (ESI-MS) $C_{18}H_{14}N_6O_5S_2$; calculated $[M+H]^+$: 459.0540; found $[M+H]^+$: 459.0554.

4-Nitro-*N*-({4-[*N*-(4-methylpyrimidin-2-yl)sulfamoyl]phenyl}carbamothioyl)benzamide (M19)

Light brown color solid, mp: 240 – 242 °C, yield 60%. ^{1}H NMR (DMSO-d_6, ppm, 400 MHz), δ 12.43 (bs, 1H, NH), 11.97 (bs, 1H, NH), 8.35 – 8.21 (m, 4H, Ar-H, NH), 8.16 (d, 2H, Ar-H, J=8.8 Hz), 8.03 (d, 2H, Ar-H, J=8.7 Hz), 7.94 (d, 2H, Ar-H, J=8.7 Hz), 6.90 (d, 1H, Ar-H, J=5.1 Hz), 2.32 (s, 3H, CH_3); ^{13}C NMR (DMSO-d_6, ppm, 100 MHz) δ 179.4 (C=S), 168.8 (C=O), 167.1, 157.9, 156.9, 150.3, 142.1, 138.5, 138.1, 130.7, 128.9, 124.1, 123.8, 115.1, 23.6; HRMS (ESI-MS) $C_{19}H_{16}N_6O_5S_2$; calculated $[M+H]^+$: 473.0696; found $[M+H]^+$: 473.0713.

4-Nitro-*N*-({4-[*N*-(4,6-dimethylpyrimidin-2-yl)sulfamoyl]phenyl}carbamothioyl)benzamide (M20)

Brown color solid, mp: 213 – 215 °C, yield 65%. ^{1}H NMR (DMSO-d_6, ppm, 400 MHz), δ 12.54 (s, 1H, NH), 12.03 (s, 1H, NH), 8.34 – 8.28 (m, 3H, Ar-H), 8.16 (d, 2H, Ar-H, J=8.7 Hz), 8.04 (d, 2H, Ar-H, J=8.6 Hz), 7.97 – 7.92 (m, 2H, Ar-H), 6.72 (s, 1H, NH), 2.25 (s, 6H, 2xCH_3); ^{13}C NMR (DMSO-d_6, ppm, 100 MHz) δ 179.4 (C=S), 167.0 (C=O), 162.7, 156.5, 150.3, 141.8, 138.4, 131.1, 129.2, 124.1, 123.9, 123.8, 113.6, 23.2; HRMS (ESI-MS) $C_{20}H_{18}N_6O_5S_2$; calculated $[M+H]^+$: 487.0853; found $[M+H]^+$: 487.0871.

General procedure for the synthesis of compounds MD1-MD4 (Scheme 1)

To a stirred solution of benzamide derivatives (M1–20) (0.5 mmol) in ethanol (10 mL) were added the ethyl bromoacetate (0.05 mL, 0.5 mmol) and sodium acetate (0.09 g, 1 mmol). The reaction mixture was refluxed for 15–24 h, and the progress of the reaction was monitored by TLC. On completion, the precipitates formed were filtered and recrystallized from ethanol to afford the products (**MD1-MD4**) (Tugrak Sakarya et al. 2023).

4-Methoxy-*N*-[4-oxo-3-(4-sulfamoylphenyl)thiazolidin-2-ylidene]benzamide (MD1)

Dark brown solid, yield: 16%. ^{1}H NMR (DMSO-d_6, ppm, 400 MHz) δ 8.02 (d, J=8.6 Hz, 2H, Ar-H), 7.84 (d, J=8.8 Hz, 2H, Ar-H), 7.68 (d, J=8.5 Hz, 2H, Ar-H), 7.54 (s, 2H, -SO_2NH_2), 6.98 (d, J=8.9 Hz, 2H, Ar-H), 4.16 (s, 2H, Ar-H), 3.81 (s, 3H, OCH_3); ^{13}C NMR (DMSO-d_6, ppm, 100 MHz) δ 175.86, 173.21, 172.99, 163.76, 144.66, 138.46, 132.01, 129.50, 127.85, 126.90, 114.38, 55.98 (OCH_3), 33.98 (-CH_2-). HRMS (ESI-MS) $C_{17}H_{15}N_3O_5S_2$, calculated $[M+H]^+$: 406.0526; found $[M+H]^+$: 406.0543.

4-Chloro-*N*-[4-oxo-3-(4-sulfamoylphenyl)thiazolidin-2-ylidene]benzamide (MD2)

Clear brown solid, yield: 15%. ^{1}H NMR (DMSO-d_6, ppm, 400 MHz) δ 8.02 (d, J=8.6 Hz, 2H, Ar-H), 7.86 (d, J=8.6 Hz, 2H, Ar-H), 7.68 (d, J=8.6 Hz, 2H, Ar-H), 7.57 – 7.50 (m, 4H, -SO_2NH_2, Ar-H), 4.19 (s, 2H, -CH_2-); ^{13}C NMR (DMSO-d_6, ppm, 100 MHz) δ 175.66, 174.92, 173.23, 144.74, 138.67, 138.29, 134.13, 131.49, 129.45, 129.30, 126.96, 34.17 (-CH_2-). HRMS (ESI-MS) $C_{16}H_{12}N_3O_4S_2Cl$, calculated $[M+H]^+$: 410.0031; found $[M+H]^+$:410.0048.

4-Bromo-*N*-[4-oxo-3-(4-sulfamoylphenyl)thiazolidin-2-ylidene]benzamide (MD3)

Orange solid, yield: 16%. ^{1}H NMR (DMSO-d_6, ppm, 400 MHz) δ 8.02 (d, J=8.4 Hz, 2H, Ar-H), 7.78 (d, J=8.4 Hz, 2H, Ar-H), 7.68 (m, 4H, Ar-H), 7.53 (s, 2H, -SO_2NH_2), 4.19 (s, 2H, -CH_2-); ^{13}C NMR (DMSO-d_6, ppm, 100 MHz) δ 175.80, 174.94, 173.22, 144.71, 138.32, 134.48, 132.26, 131.61, 129.45, 127.89, 126.95, 34.18 (-CH_2-); HRMS (ESI-MS) $C_{16}H_{12}N_3O_4SBr$, calculated $[M+H]^+$: 453.9525; found $[M+H]^+$: 453.9536.

4-Fluoro-*N*-[4-oxo-3-(4-sulfamoylphenyl)thiazolidin-2-ylidene]benzamide (MD4)

Brown solid, yield: 20%. ^{1}H NMR (DMSO-d_6, ppm, 400 MHz) δ 8.03 (d, J=8.6 Hz, 2H, Ar-H), 7.93 (dd, J=8.7, 5.7 Hz, 2H, Ar-H), 7.68 (d, J=8.6 Hz, 2H, Ar-H), 7.52 (s, 2H, -SO_2NH_2), 7.29 (t, J=8.7 Hz, 2H, Ar-H), 4.19 (s, 2H, -CH_2-); ^{13}C NMR (DMSO-d_6, ppm, 100 MHz) δ 175.48, 174.50, 173.23, 166.83, 164.38, 144.73, 132.57 (d, J_{CF}=9.8 Hz), 131.96 (d, J_{CF}=2.5 Hz), 129.46, 126.95, 116.20 (d, J_{CF}=22 Hz), 34.11; HRMS (ESI-MS) $C_{16}H_{12}N_3O_4FS_2$, calculated $[M+H]^+$: 394.0326; found $[M+H]^+$: 394.0341.

Carbonic anhydrase enzyme assay

Human CA isoforms (hCAI and hCAII) were isolated using the sepharose −4B - L - tyrosine sulfanilamide affinity segregation process, as previously reported. Protein concentrations were measured using the Bradford method at 595 nm (Bradford 1976). The compounds' inhibitory effects were studied by measuring esterase activity in accordance with Verpoorte et al., as described in prior investigations (Verpoorte et al. 1967). The hCA activity was evaluated by monitoring the conversion of the *p*-nitrophenyl acetate substrate to p-nitro phenolate at 348 nm using a spectrophotometer (UV-VIS Spectrophotometer, UV mini-1240, Shimadzu Corporation). Acetazolamide (AZA) was utilized as the control medication. The Lineweaver-Burk plot was used to

determine the drugs' inhibition constants (Ki). Lineweaver–Burk graphics are presented as a supplementary file (Tugrak et al. 2021a, c; Kocyigit et al. 2017; Bradford 1976; Verpoorte et al. 1967).

Acetylcholinesterase enzyme assay

The effects of compounds on AChE enzyme were investigated. Two substrates which are 5,5-dithiobis(2-nitrobenzoic acid) (DTNB) and acetylcholiniodate (AChI) were used in the inhibition tests. In addition, Tris / HCl (100 ml, 1 M, pH = 8) buffer was used in this method for AChE enzyme. The final volume was completed to 100 µL and changes in the absorption were followed at 412 nm. The IC_{50} values of the compounds were calculated via activity (%) versus compounds concentration plots (See supplementary file) (Tugrak et al. 2021a; El-Sayed et al. 2019).

α-Glycosidase enzyme assay

α-Glycosidase inhibition effect of the compounds (**M1-M20**, and **MD1-MD4**) was made according to the method of Tao et al. (Tao et al. 2013). *p*-Nitrophenyl-D-glucopyranoside (p-NPG) was used as substrate. First, 75 µL of phosphate buffer solution (5 mM, pH 7.4) was added to 20 µL of α-glycosidase solution (0.15EU/mL), which was prepared in phosphate buffer (pH 7.4, 5 mM) and 5 µLof different concentrations of the compounds. Then, it was preincubated at 35 °C for 10 min before adding p-NPG to initiate the reaction. Also, 20 µL of p-NPG was transferred in phosphate buffer (pH 7.4, 5 mM) after a short incubation period at 35 °C. The absorbances were measured at 405 nm. One α-glycosidase unit is the quantity of enzyme that catalyzes the hydrolysis of 1.0 mol p-NPG per minute at pH 7.4.

α-Amylase enzyme assay

α-Amylase inhibitory effects of the compounds (**M1-M20**, and **MD1-MD4**) were realized according to the procedure of Xiao using starch as substrate (Xiao et al. 2006). For starch preparation, 0.4 M starch mixture was prepared in 80 mL NaOH solution at 80 °C for 30 min. Then, 35 µL of starch solution, 35 µL of phosphate buffer (pH 6.9), and 10 µL of different concentrations of the compounds were mixed and incubated at 35 °C for 25 min. Lastly, 20 µL of the α-amylase solution was added to the final mixture and reincubated for 25 min. The reactions were finished by adding 50 µL of HCl (0.1 M) to each tube. The absorbance was measured at 580 nm. One α-amylase unit is defined as the quantity of α amylase required to release 1 µmol of reducing sugar estimated as glucose per min (pH 6.9, 40 °C). (Turker et al. 2018).

Computational method

In silico docking analyses were conducted using the AutoDock Vina program (Trott and Olson 2010). The molecular structures of **M1**, **M9**, **M10**, and **M17** were optimized in their ground-state and gas-phase configurations through Density Functional Theory (DFT) calculations, employing the B3LYP functional and the 6-311 + + G(d, p) basis set via the Gaussian 09 W software package (Frisch et al. 2009). Three-dimensional visualizations of the optimized structures were produced using the GaussView program (Dennington et al. 2009), with no symmetry constraints applied. In the final section, Molecular Electrostatic Potential (MEP) analysis of the **M1**, **M9**, **M10**, and **M17** molecules was conducted using the checkpoint (.chk) files. This analysis enabled the identification of electrophilic and nucleophilic regions within these molecules.

Supplementary Information The online version contains supplementary material available at https://doi.org/10.1007/s11696-026-04771-z.

Acknowledgements The authors are thankful to Prof. Dr. C. Kazaz and Dr. B. Anil (Ataturk University) for NMRs, Ataturk Universitesi BAP Office (BAP project No: 2021/8919) and Tokat Gaziosmapasa University BAP Office (BAP project No: 2022/84) for their financial support and Dr. Serkan Levent (Anadolu University) for HRMS, Prof. Dr. Fatih UCUN for his helpful contribution for Gaussian calculations.

Author contribution Sakarya MT: Synthesis of target compounds, investigation, characterization of compounds, writing original draft and final approval of the completed article. Gul HI, Gul M: Contributed to the project supervision, Yamali C: synthesis of target compounds, investigation, characterization of compounds, writing and final approval of the completed article, Sert Y: Molecular Docking, Erturk A, and Gulcin I: Validation of biological activities assay.

Funding Open access funding provided by the Scientific and Technological Research Council of Türkiye (TÜBİTAK).

Declarations

Conflict of interest The authors report no conflict of interest and are responsible for the contents and writing of the paper.

Open Access This article is licensed under a Creative Commons Attribution 4.0 International License, which permits use, sharing, adaptation, distribution and reproduction in any medium or format, as long as you give appropriate credit to the original author(s) and the source, provide a link to the Creative Commons licence, and indicate if changes were made. The images or other third party material in this article are included in the article's Creative Commons licence, unless indicated otherwise in a credit line to the material. If material is not included in the article's Creative Commons licence and your intended use is not permitted by statutory regulation or exceeds the permitted use, you will need to obtain permission directly from the copyright holder. To view a copy of this licence, visit http://creativecommons.org/licenses/by/4.0/.

References

Aleid G, Imran M, Ullah H, Taha M, Khan J, Rahim F et al (2024) Design, synthesis, in vitro bio-evaluation and in silico molecular docking study of benzohydrazide based thiourea analogues. Results Chem 11:101756. https://doi.org/10.1016/j.rechem.2024.101756

Alterio V, Di Fiore A, D'Ambrosio K, Supuran CT, De Simone G (2012) Multiple binding modes of inhibitors to carbonic anhydrases: how to design specific drugs targeting 15 different isoforms? Chem rev 112(8):4421–4468. https://doi.org/10.1021/cr200176r

Arif S, Khan S, Iqbal T, Yallur BC, Rahim F, Hussain R et al (2024) Synthesis, characterization, DFT, AMDET and molecular docking reveals the binding mechanism of hydroxyl containing bis-Schiff base derivatives: An approach toward Alzheimer disease. Results Chem 10:101706. https://doi.org/10.1016/j.rechem.2024.101706

Azhar Hussain BA, PharmD MBA, PharmD JB (2023) Side effects of drugs used in the treatment of Alzheimer's disease. Side Eff Drugs Annual 45:27–32. https://doi.org/10.1016/bs.seda.2023.08.018

Becke AD (1993) Densityfunctional thermochemistry. III. the role of exact exchange. J Chem Phys 98(7):5648–5652. https://doi.org/10.1063/1.464913

Bradford MM (1976) A rapid and sensitive method for the quantitation of microgram quantities of protein utilizing the principle of protein-dye binding. Anal Biochem 72:248–254. https://doi.org/10.1016/0003-2697(76)90527-3

Buchanan D, Pham AM, Singh SK, Panda SS (2023) Molecular hybridization of alkaloids using 1,2,3-triazole-based click chemistry. Molecules 28(22):7593

Carta F, Supuran CT, Scozzafava A (2014) Sulfonamides and their isosters as carbonic anhydrase inhibitors. Future Med Chem 6(10):1149–1165. https://doi.org/10.4155/fmc.14.68

Ch'ng LZ, Barakatun-Nisak MY, Zukiman WZHW, Abas F, Wahab NA (2019) Nutritional strategies in managing postmealglucose for type 2 diabetes: A narrative review. Diabetes Metab Syndr 13(4):2339–2345. https://doi.org/10.1016/j.dsx.2019.05.026

Chen X-L, Zhang K, Zhao X, Wang H-L, Han M, Li R, Zhang Z-N, Zhang Y-M (2023) Triterpenoids from Kochiae Fructus: glucose uptake in 3T3-L1 adipocytes and α-glucosidase inhibition, in silico molecular docking. Int J Mol Sci 24(3):2454. https://doi.org/10.3390/ijms24032454

Chiasson JL, Josse RG, Gomis R, Hanefeld M, Karasik A, Laakso M (2002) Acarbose for prevention of type 2 diabetes mellitus: TheSTOP-NIDDM randomised trial. Lancet (North Am Edition) 359(9323):2072–2077. https://doi.org/10.1016/S0140-6736(02)08905-5

Christos V, Rizos A, Kei, Elisaf MS (2016) The current role of thiazolidinediones in diabetes management. Arch Toxicol 90(8):1861–1881. https://doi.org/10.1007/s00204-016-1737-4

Coric V, Salloway S, van Dyck CH, Dubois B, Andreasen N, Brody M (2015) Targeting prodromal Alzheimer disease with avagacestat: a randomized clinical trial. JAMA Neurol 72:1324–1333. https://doi.org/10.1001/jamaneurol.2015.0607

Daina A, Michielin O, Zoete V (2017) SwissADME: a free web tool to evaluate pharmacokinetics, drug-likeness and medicinal chemistry friendliness of small molecules. Sci Rep 7:42717. https://doi.org/10.1038/srep42717

Dennington R, Keith T, Millam J (2009) GaussView, version 5, Semichem Inc. Shawnee Mission, KS

Douros A, Yin H, Yu OHY, Filion KB, Azoulay L, Suissa S (2017) Pharmacologic differences of sulfonylureas and the risk of adverse cardiovascular and hypoglycemic events. Diabetes Care 40(11):1506–1513. https://doi.org/10.2337/dc17-0595

Efeoglu C, Yetkin D, Nural Y, Ece A, Seferoglu Z, Ayaz F (2022) Novel urea-thiourea hybrids bearing 1,4-naphthoquinone moiety: Anti-inflammatory activity on mammalian macrophages by regulating intracellular PI3K pathway, and molecular docking study. J Mol Struct 1264:133284. https://doi.org/10.1016/j.molstruc.2022.133284

El-Sayed NA, Farag AE, Ezzat MAF, Akincioglu H, Gulcin I, Abou-Seri SM (2019) Design, synthesis, in vitro and in vivo evaluation of novel pyrrolizine-based compounds with potential activity as cholinesterase inhibitors and anti-Alzheimer's agents. Bioorg Chem 93:103312. https://doi.org/10.1016/j.bioorg.2019.103312

Ellman GL, Courtney KD, Andres VJ, Featherstone RM (1961) A new and rapid colorimetric determination of acetylcholinesterase activity. Biochem Pharm 7:88–95. https://doi.org/10.1016/0006-2952(61)90145-9

Ferreira LG, Dos Santos RN, Oliva G, Andricopulo AD (2015) Molecular docking and structure-based drug design strategies. Molecules 20(7):13384–13421. https://doi.org/10.3390/molecules200713384

Frisch MJ, Trucks G, Schlegel H, Scuseria G, Robb M, Cheeseman J, Scalmani G, Barone V, Mennucci B, Petersson G (2009) Gaussian 09, Revision D, vol 01. Gaussian, Inc., Wallingford, CT

Gamal MA, Fahim SH,Giovannuzzi S, Fouad MA, Bonardi A, Grattari P et al (2024) Probing benzenesulfonamide-thiazolidinone hybrids as multitarget directed ligands for efficient control of type 2 diabetes mellitus through targeting the enzymes: alpha-glucosidase and carbonic anhydrase II. Eur Med Chem 271:116434. https://doi.org/10.1016/j.ejmech.2024.116434

Gupta VB, Gupta VK, Martins R (2013) Semagacestat for treatment of Alzheimer's disease. N Engl J Med 369:1660–1661. https://doi.org/10.1056/NEJMc131084

Hayat S, Ullah H, Rahim F, Ullah I, Taha M, Iqbal N et al (2023) Synthesis, biological evaluation and molecular docking study of benzimidazole derivatives as α-glucosidase inhibitors and anti-diabetes candidates. J Mol Struct 1276:134774. https://doi.org/10.1016/j.molstruc.2022.134774

Imbimbo BP, Watling M (2019) Investigational BACE inhibitors for the treatment of Alzheimer's disease. Expert Opin Investig Drugs 28(11):967–975. https://doi.org/10.1080/13543784.2019.1683160

Iqbal T, Khan S, Rahim F, Tayyab M, Hussain R, Khan Y et al (2025) Insights into the role of potent thiadiazole based Schiff base derivatives in targeting type-II diabetes: a combine in-vitro and in-silico approaches. J Mol Struct 1321(3):140000. https://doi.org/10.1016/j.molstruc.2024.140000

Ivanova J, Leitans J, Tanc M, Kazaks A, Zalubovskis R, Supuran CT, Tars K (2015) X-ray crystallography-promoted drug design of carbonic anhydrase inhibitors. Chem Commun 51(33):7108–7111. https://doi.org/10.1039/C5CC01854D

Kannan K, Ramanadham M, Jones T (1984) Structure, refinement, and function of carbonic anhydrase isozymes: refinement of human carbonic anhydrase I. Annals New York Acad Sci 429(1):49–60. https://doi.org/10.1111/j.1749-6632.1984.tb12314.x

Khan M, Patujo J, Mushtaq I, Ishtiag A, Tahir MN, Bibi S et al (2022) Anti-diabetic potential, crystal structure, molecular docking, DFT, and optical-electrochemical studies of new dimethyl and diethyl carbamoyl-N, N′-disubstituted based thioureas. J Mol Struct 1253:132207. https://doi.org/10.1016/j.molstruc.2021.132207

Khan Y, Khan S, Rehman W, Hussain R, Maalik A, Ali F et al (2023a) Hybrid molecules of thiadiazole-based benzothioate and benzenesulfonothioate: synthesis, structural analysis, and evaluation as potential inhibitors of thymidine phosphorylase and β-glucuronidase through in vitro and in silico approaches. J Mol

Struc 1294(2):136439. https://doi.org/10.1016/j.molstruc.2023.136439
Khan Y, Khan S, Hussain R, Rehman W, Maalik A, Gulshan U et al (2023b) Identification of indazole-based Thiadiazole-bearing thiazolidinone hybrid derivatives: theoretical and computational approaches to develop promising anti-Alzheimer's candidates. Pharmaceuticals 16(12):1667. https://doi.org/10.3390/ph16121667
Khan S, Hussain R, Khan Y, Iqbal T, Chinnam S, Akif M et al (2024) Hybrid benzothiazole derived fused triazole/thiazole derivatives as versatile anti-Alzheimer agents: synthesis, characterization, biological evaluation and molecular docking studies. J Mol Struc 1318(2):139200. https://doi.org/10.1016/j.molstruc.2024.139200
Kocyigit UM, Budak Y, Gurdere MB, Tekin Ş, Köprülü TK, Erturk F et al (2017) Synthesis, characterization, anticancer, antimicrobial and carbonic anhydrase inhibition profiles of novel (3aR,4S,7R,7aS)-2-(4-((E)-3-(3-aryl)acryloyl) phenyl)-3a,4,7,7a-tetrahydro-1H-4,7-methanoisoindole-1,3(2H)-dione derivatives. Bioorg Chem 70:118–125. https://doi.org/10.1016/j.bioorg.2016.12.001
Kokil GR, Rewatkar PV, Verma A, Thareja S, Naik SR (2010) Pharmacology and chemistry of diabetes mellitus and antidiabetic drugs: a critical review. Curr Med Chem 17:4405–4423. https://doi.org/10.2174/092986710793361225
Krishnan R, Binkley JS, Seeger R, Pople JA (1980) Self-consistent molecular orbital methods. XX. A basis set for correlated wave functions. J Chem Phys 72(1):650–654. https://doi.org/10.1063/1.438955
Kryger G, Silman I, Sussman JL (1999) Structure of acetylcholinesterase complexed with E2020 (Aricept®): implications for the design of new anti-Alzheimer drugs. Structure 7(3):297–307. https://doi.org/10.1016/S0969-2126(99)80040-9
Kulabaş N, Özakpınar ÖB, Özsavcı D, Leyssen P, Neyts J, Kucukguzel I (2017) Synthesis, characterization and biological evaluation of thioureas, acylthioureas and 4-thiazolidinones as anticancer and antiviral agents. Marmara Pharm J 21(2):371–384. https://doi.org/10.12991/marupj.300913
Lemon N, Canepa E, Ilies MA, Fossati S (2021) Carbonic anhydrases as potential targets against neurovascular unit dysfunction in Alzheimer's disease and stroke. Front Aging Neurosci 16:13:772278. https://doi.org/10.3389/fnagi.2021.772278
Lipinski CA (2000) Drug-like properties and the causes of poor solubility and poor permeability. J Pharmacol Toxicol Methods 44(1):235–249. https://doi.org/10.1016/S1056-8719(00)00107-6
Lopez A, Siddiqi FH, Villeneuve J, Ureshino RP, Jeon HY, Koulousakis P, Keeling S, McEwan WA, Fleming A, Rubinsztein DC (2025) Carbonic anhydrase inhibition ameliorates tau toxicity via enhanced tau secretion. Natu Chem Biol 21:577–587. https://doi.org/10.1038/s41589-024-01762-7
Lou Y, McDonald PC, Oloumi A, Chia S, Ostlund C, Ahmadi A et al (2011) Targeting tumor hypoxia: suppression of breast tumor growth and metastasis by novel carbonic anhydrase IX inhibitors. Cancer Res 71(9):3364–3376. https://doi.org/10.1158/0008-5472.CAN-10-4261
Mahdavi M, Shirazi MS, Taherkhani R, Saeedi M, Alipour E, Moghadam FH et al (2014) Synthesis, biological evaluation and docking study of 3-aroyl-1-(4-sulfamoylphenyl)thiourea derivatives as 15-lipoxygenase inhibitors. Eur J Med Chem 82:308–313. https://doi.org/10.1016/j.ejmech.2014.05.054
Mahmudov I, Demir Y, Sert Y, Abdullayev Y, Sujayev A, Alwasel SH, Gulcin I (2022) Synthesis and inhibition profiles of N-benzyl- and N-allyl aniline derivatives against carbonic anhydrase and acetylcholinesterase-A molecular docking study. Arab J Chem 15(3):103645. https://doi.org/10.1016/j.arabjc.2021.103645
Marucci G, Buccioni M, Ben DD, Lambertucci C, Volpini R, Amenta F (2021) Efficacy of acetylcholinesterase inhibitors in Alzheimer's disease. Neuropharmacol 190:108352. https://doi.org/10.1016/j.neuropharm.2020.108352
Mary T, Korytkowski MD (2004) Sulfonylurea treatment of type 2 diabetes mellitus: focus on glimepiride. Pharmacother 24(5):606–620
Meng X-Y, Zhang H-X, Mezei M, Cui M (2011) Molecular docking: a powerful approach for structure-based drug discovery. Curr Comput-Aided Drug Des 7(2):146–157. https://doi.org/10.2174/157340911795677602
Mert S, Demir Y, Sert Y, Kasımoğulları R, Gulcin I (2025) Synthesis, biological evaluation and molecular docking of novel pyrazole derivatives as multitarget acetylcholinesterase and carbonic anhydrase inhibitors. J Mol Struc 1319:139472. https://doi.org/10.1016/j.molstruc.2024.139472
Mesiti F, Chavarria D, Gaspar A, Alcaro S, Borges F (2019) The chemistry toolbox of multitarget-directed ligands for Alzheimer's disease. Eur J Med Chem 1:181:111572. https://doi.org/10.1016/j.ejmech.2019.111572
Murray JS, Politzer P (2011) The electrostatic potential: an overview. Comput Mol Sci 1(2):153–163. https://doi.org/10.1002/wcms.19
Nanjan MJ, Mohammed M, Prashantha Kumar BR, Chandrasekar MJN (2018) Thiazolidinediones as antidiabetic agents: a critical review. Bioorg Chem 77:548–567. https://doi.org/10.1016/j.bioorg.2018.02.009
Neri D, Supuran CT (2011) Interfering with pH regulation in tumours as a therapeutic strategy. Nat Rev Drug Discov 10(10):767–777
Nunes D, Loureiro JA, Pereira MC (2022) Drug Delivery Systems as a Strategy to Improve the Efficacy of FDA-Approved Alzheimer's. Drugs Pharm 14(11):2296. https://doi.org/10.3390/pharmaceutics14112296
Pacchiano F, Aggarwal M, Avvaru BS, Robbins AH, Scozzafava A, McKenna R et al (2010) Selective hydrophobic pocket binding observed within the carbonic anhydrase II active site accommodate different 4-substituted-ureido-benzenesulfonamides and correlate to inhibitor potency. Chem Commun 46(44):8371–8373. https://doi.org/10.1039/c0cc02707c
Pacchiano F, Carta F, McDonald PC, Lou Y, Vullo D, Scozzafava A et al (2011) Ureido-substituted benzenesulfonamides potently inhibit carbonic anhydrase IX and show antimetastatic activity in a model of breast cancer metastasis. J Med Chem 54(6):1896–1902. https://doi.org/10.1021/jm101541x
Pathak C, Kabra UD (2024) A comprehensive review of multi-target directed ligands in the treatment of Alzheimer's disease. Bioorg Chem 144:107152. https://doi.org/10.1016/j.bioorg.2024.107152
Politzer P, Truhlar DG (2013) Chemical applications of atomic and molecular electrostatic potentials: reactivity, structure, scattering, and energetics of organic, inorganic, and biological systems. Springer Science & Business Media
Protein data Bank, Berman M, Westbrook J, Feng Z, Gilliland G, Bhat TN, Weissig H, Shindyalov IN, Bourne PE (2000) The Protein Data Bank. Nucleic Acids Res 28:235–242. https://www.rcsb.org/.H https://doi.org/10.1093/nar/28.1.235
Rizos CV, Kei A, Elisaf MS (2016) The current role of thiazolidinediones in diabetes management. Arch Toxicol 90(8):1861–1881. https://doi.org/10.1007/s00204-016-1737-4
Saleh BHO (2024) Using bioinformatics tools to detect the effect of smoking on the α-amylase enzyme, AIP Conference Proceedings, AIP Publishing
Saltos MBV, Puente BFN, Faraone I, Milella L, Tommasi N, De, Braca A (2015) Inhibitors of α-amylase and α-glucosidase from Andromachia igniaria Humb. Bonpl Phytochem Lett 14:45–50. https://doi.org/10.1016/j.phytol.2015.08.018
Scientific Software http://www.3dsbiovia.com/.BIOVIA Discovery Studio. D. SYSTÈMES (2016) Description. Discovery … software. Cite this publication. BibTeX EndNote. APA Chicago DIN 1505. Harvard

Solesio ME, Peixoto PM, Debure L, Madamba SM, de Leon MJ, Wisniewski T, Pavlov EV, Silvia Fossati S (2018) Carbonic anhydrase inhibition selectively prevents amyloid β neurovascular mitochondrial toxicity. Aging Cell 17(4):e12787. https://doi.org/10.1111/acel.12787

Supuran CT (2018) Carbon- versus sulphur-based zinc binding groups for carbonic anhydrase inhibitors? J Enzyme Inhib Med Chem 33(1):485–495. https://doi.org/10.1080/14756366.2018.1428572

Tao Y, Zhang Y, Cheng Y, Wang Y (2013) Rapid screening and identification of alpha-glucosidase inhibitors from mulberry leaves using enzyme-immobilized magnetic beads coupled with HPLC/MS and NMR. Biomed Chromatog 27(2):148–155. https://doi.org/10.1002/bmc.2761

Taslimi P, Aslan HE, Demir Y, Oztaskin N, Maras A, Gulcin I et al (2018) Diarylmethanon, bromophenol and diarylmethane compounds: Discovery of potent aldose reductase, alpha-amylase and alpha-glycosidase inhibitors as new therapeutic approach in diabetes and functional hyperglycemia. Int J Biol Macromol 119:857–863. https://doi.org/10.1016/j.ijbiomac.2018.08.004

Taylor RD, Jewsbury PJ, Essex JW (2002) A review of protein-small molecule docking methods. J Comput-Aided Mol Des 16:151–166. https://doi.org/10.1023/a:1020155510718

Trott O, Olson AJ (2010) AutoDock Vina: improving the speed and accuracy of docking with a new scoring function, efficient optimization, and multithreading. J Comput Chem 31(2):455–461. https://doi.org/10.1002/jcc.21334

Tugrak M, Gul HI, Anil B, Gulcin I (2020) Synthesis and pharmacological effects of novel benzenesulfonamides carrying benzamide moiety as carbonic anhydrase and acetylcholinesterase inhibitors. Turkish J Chem 44(6):1601–1609. https://doi.org/10.3906/kim-2007-37

Tugrak M, Gul HI, Demir Y, Levent S, Gulcin I (2021a) Synthesis and in vitro carbonic anhydrases and acetylcholinesterase inhibitory activities of novel imidazolinone-based benzenesulfonamides. Arch Pharm 354(4):e2000375. https://doi.org/10.1002/ardp.202000375

Tugrak M, Gul HI, Sakagami H, Kaya R, Gulcin I (2021b) Synthesis and biological evaluation of new pyrazolebenzene-sulphonamides as potential anticancer agents and hCA I and II inhibitors. Turkish J Chem 45(3):528–539. https://doi.org/10.3906/kim-2009-37

Tugrak M, Gul HI, Demir Y, Gulcin I (2021c) Synthesis of benzamide derivatives with thiourea-substituted benzenesulfonamides as carbonic anhydrase inhibitors. Arch Pharm 354(2):e2000230. https://doi.org/10.1002/ardp.202000230

Tugrak Sakarya M, Gul HI, Yamali C, Taslimi P, Taskin Tok T (2023) Molecular docking studies and biological activities of benzenesulfonamide-based thiourea and thiazolidinone derivatives targeting cholinesterases α-glucosidase and α-amylase enzymes. J Turkish Chem Soc Sect A: Chem 10(2):385–424. https://doi.org/10.18596/jotcsa.1111172

Turker F, Barut Celepci D, Aktas A, Taslimi P, Gök Y, Aygün M et al (2018) meta-Cyanobenzyl substituted benzimidazolium salts: Synthesis, characterization, crystal structure and carbonic anhydrase, alpha-glycosidase, butyrylcholinesterase, and acetylcholinesterase inhibitory properties. Arch Pharm 351(7):e1800029. https://doi.org/10.1002/ardp.20180002996

Ullah H, Uddin I, Rahim F, Khan F, Sobia, Taha M et al (2022) In vitro α-glucosidase and α-amylase inhibitory potential and molecular docking studies of benzohydrazide based imines and thiazolidine-4-one derivatives. J Mol Struc 1251:132058. https://doi.org/10.1016/j.molstruc.2021.132058

Verpoorte JA, Mehta S, Edsall JT (1967) Esterase activities of human carbonic anhydrases B and C. J Biol Chem 242(18):4221–4229

Viegas-Junior C, Danuello A, da Silva Bolzani V, Barreiro EJ, Fraga CA (2007) Molecular hybridization: a useful tool in the design of new drug prototypes. Curr Med Chem 14(17):1829–1852. https://doi.org/10.2174/092986707781058805

Xiao Z, Storms R, Tsang A (2006) A quantitative starch-iodine method for measuring alpha-amylase and glucoamylase activities. Anal Biochem 351(1):146–148. https://doi.org/10.1016/j.ab.2006.01.036

Yamali C, Sevin S, Nenni M, Tugrak Sakarya M, Uyar R, Aygul A et al (2023) Design, synthesis, and assessment of pharmacological properties of indole-based fluorinated chalcones and their benzenesulfonamide analogs. Chem Papers 77(12):7903–7918. https://doi.org/10.1007/s11696-023-03060-3

Yang G, Zhou R, Guo X, Yan C, Lei J, Shi Y (2021) Structural basis of γ-secretase inhibition and modulation by small molecule drugs. Cell 184(2):521–533. https://doi.org/10.1016/j.cell.2020.11.049

Zada H, Ullah H, Hayat S, Rahim F, Khan F, Wadood A (2022) Synthesis of triazinoindole bearing sulfonamide derivatives, in vitro α-amylase activity and their molecular docking study. Chem Data Collect 39:100875. https://doi.org/10.1016/j.cdc.2022.100875

Zahra U, Saeed A, Abdul Fattah T, Florke U, Erben MF (2022) Recent trends in chemistry, structure, and various applications of 1-acyl-3-substituted thioureas: a detailed review. RSC Adv 12(20):12710–12745. https://doi.org/10.1039/D2RA01781D

Zhang J, Zhang Y, Wang J, Xia Y, Chen JZ L (2024) Recent advances in Alzheimer's disease: mechanisms, clinical trials and new drug development strategies. Sig Transduct Targ Ther 9(211):1–35. https://doi.org/10.1038/s41392-024-01911-3

Publisher's note Springer Nature remains neutral with regard to jurisdictional claims in published maps and institutional affiliations.